Redox Biology 79 (2025) 103468

Contents lists available at ScienceDirect

Redox Biology

journal homepage: www.elsevier.com/locate/redox

Liraglutide and GLP-1(9–37) alleviated hepatic ischemia-reperfusion injury by inhibiting ferroptosis via GSK3β/Nrf2 pathway and SMAD159/Hepcidin/FTH pathway

Chenqi Lu [a], Cong Xu [b], Shanglin Li [c], Haiqiang Ni [a,*], Jun Yang [a,**]

[a] Institute of Organ Transplantation, Tongji Hospital, Tongji Medical College, Huazhong University of Science and Technology, Ministry of Education, NHC Key Laboratory of Organ Transplantation, Key Laboratory of Organ Transplantation, Chinese Academy of Medical Sciences, Wuhan, China
[b] Division of Nephrology, Department of Internal Medicine, Tongji Hospital, Tongji Medical College, Huazhong University of Science and Technology, Wuhan, China
[c] Department of General Surgery, Wuhan Children's Hospital, Tongji Medical College, Huazhong University of Science and Technology, Wuhan, China

ARTICLE INFO

Keywords:
Liraglutide
Ischemia-reperfusion injury
GLP-1(9–37)
Ferroptosis

ABSTRACT

Ferroptosis plays a pivotal role in the pathogenesis of ischemia-reperfusion injury (IRI). Liraglutide, as a GLP-1 receptor (GLP-1R) agonist, has exhibited extensive biological effects beyond its hypoglycemic action. Recent studies have shed light on the regulatory influence of Liraglutide on ferroptosis, yet the precise underlying mechanism remains elusive. GLP-1(9–37), as a metabolite of GLP-1, has a low affinity to GLP-1R. Its effect on ferroptosis remains unknown. In this study, we investigated the effects of Liraglutide and GLP-1(9–37) on the ferroptosis during hepatic ischemia-repferfusion (I/R), as well as the underlying specific mechanisms. We found that the administration of Liraglutide alleviated I/R-induced liver injury with less iron accumulation and lower lipid peroxidation, which was not entirely dependent on the presence of GLP-1R. Similarly, GLP-1(9–37) also exhibited these effects. Besides, both of them increased GPX4 expression and decreased COX2 expression. These effects were reversed by a High-Iron Diet. In vitro study showed similar results. In mechanism study, we found that both Liraglutide and GLP-1(9–37) treatment promoted the nuclear translocation of Nrf2 by inhibiting GSK-3β, thereby reducing lipid peroxides. Furthermore, they increased FTH and FTL expression via the SMAD159/Hepcidin pathway, which contributed to the decreased iron accumulation. In conclusion, this study determined that both Liraglutide and GLP-1(9–37) alleviated hepatic ischemia-reperfusion injury (HIRI) by suppressing ferroptosis via the activation of the GSK3β/Nrf2 pathway and the SMAD159/Hepcidin/FTH pathway.

1. Introduction

Ischemia-Reperfusion Injury (IRI) embodies a multifaceted pathological phenomenon, characterized by the deprivation of oxygen and depletion of ATP during the ischemic phase, coupled with the emergence of a myriad of inflammatory mediators and reactive oxygen species (ROS) during reperfusion. Within this intricate cascade, a diverse array of cellular demise pathways are set into motion, encompassing apoptosis, autophagy, pyroptosis, and ferroptosis, among others [1–3]. Hepatic Ischemia-Reperfusion Injury (HIRI) represents an inevitable consequence following hepatic procedures such as partial hepatectomy and liver transplantation [4]. Severe HIRI can lead to delayed graft function, acute or chronic rejection, hepatic dysfunction, and even failure, posing a serious threat to the lives of patients. However, due to the intricate nature of the injury mechanisms, a definitive and efficacious preventive strategy for HIRI remains elusive [5]. Therefore, it is necessary to understand the pathogenesis of HIRI and explore the targeted therapeutic drugs.

Ferroptosis is an emerging form of programmed cell death orchestrated by iron-dependent lipid peroxidation [6]. The substantial accumulation of iron and lipid peroxidation are the primary hallmarks of ferroptosis [7]. Cells undergoing ferroptosis exhibit distinctive morphological features, including mitochondrial shrinkage and heightened mitochondrial membrane density, setting them apart from other

* Corresponding author. Institute of Organ Transplantation, Tongji Hospital, Tongji Medical College, Huazhong University of Science and Technology, 1095 Jiefang Avenue, Wuhan, 430030, China.
** Corresponding author. Institute of Organ Transplantation, Tongji Hospital, Tongji Medical College, Huazhong University of Science and Technology, 1095 Jiefang Avenue, Wuhan, 430030, China.
E-mail addresses: nhq6248@126.com (H. Ni), jy@tjh.tjmu.edu.cn (J. Yang).

https://doi.org/10.1016/j.redox.2024.103468
Received 10 November 2024; Received in revised form 7 December 2024; Accepted 11 December 2024
Available online 12 December 2024

modes of cell death [6,7]. Within the cellular environment, an excess of iron triggers the activation of an array of oxidases and the production of a substantial quantity of reactive oxygen species (ROS) through the Fenton reaction, consequently inducing the peroxidation of polyunsaturated fatty acids on the cell membrane. Simultaneously, if the antioxidant defense system is compromised, hindering the elimination of accumulated lipid peroxides, ferroptosis will ensue [8–10]. Ferroptosis plays a pivotal role in the pathogenesis of numerous diseases. Studies indicates that an excess of iron may serve as a risk factor exacerbating IRI in liver transplantation [11,12]. Following ischemia-reperfusion (I/R), mice livers demonstrate a substantial accumulation of iron and lipid peroxides. Administering a high-iron diet exacerbates the liver injury induced by I/R, whereas the application of ferroptosis inhibitors effectively mitigates hepatic pathological damage and lowers the levels of alanine transaminase (ALT) and aspartate transaminase (AST) in serum [11,13]. Therefore, ferroptosis emerges as a promising therapeutic target for ameliorating HIRI.

Liraglutide, a long-acting GLP-1R agonist, has garnered widespread utilization in the clinical management of type 2 diabetes and obesity attributed to its profound hypoglycemic and weight loss properties [14,15]. Beyond these applications, recent basic and clinical studies have highlighted the significant protective effects of Liraglutide in various other conditions, including cardiovascular complications, kidney, liver, and nervous system diseases [16–19]. The actions of Liraglutide are also diverse. Studies have found that Liraglutide has obvious anti-inflammatory and antioxidant effects. It can inhibit the activation of the classical NF-κB inflammatory pathway and reduce the occurrence of pyroptosis by inhibiting the NLRP3 pathway [20,21]. In addition, Liraglutide can also promote the nuclear translocation of Nrf2, which can increase the expression of antioxidant enzymes such as HO-1, thereby alleviating the oxidative damage [22]. Recently, it has been reported that long-term intraperitoneal injection of Liraglutide reduced the iron content and changed the expression levels of transferrin receptor 1 (TfR1) and ferroportin (FPN) in the liver of type 2 diabetic mice, suggesting that Liraglutide may have an inhibitory effect on ferroptosis [23]. However, whether Liraglutide has an effect on the ferroptosis that occurs during hepatic ischemia-reperfusion is still unclear.

Although Liraglutide is a GLP-1R agonist, several studies have found that part of its effects are not mediated by GLP-1R, suggesting the existence of a GLP-1R-independent pathway for its actions [24,25]. One possible explanation for the GLP-1R-independent effects of GLP-1R agonists, like Liraglutide, is the presence of GLP-1 metabolites [24,26]. Under the action of dipeptidyl peptidase IV and neutral endopeptidase, GLP-1 (7–37), the active form of GLP-1, can be cleaved into GLP-1 (9–37) and GLP-1 (28–37), which have a low affinity for GLP-1R [26–28]. However, GLP-1(9–37) and GLP-1(28–37) can still attenuate disease damage in the absence of GLP-1R [24,29]. Additionally, compared with liraglutide, the metabolites also have the characteristics of no weight loss and rapid action [24].

At present, the specific mechanisms by which Liraglutide and its metabolites alleviate HIRI has not been fully elucidated. Based on the above findings, we hypothesized that Liraglutide and its metabolites may alleviate HIRI by inhibiting the occurrence of ferroptosis during hepatic ischemia-reperfusion. In this study, we examined the inhibitory effects of Liraglutide and its metabolites on ferroptosis in HIRI. Additionally, we explored whether they have regulatory effects on lipid peroxidation and iron homeostasis, respectively.

2. Methods

2.1. Animals

Male C57BL/6 mice, six to eight weeks old, were purchased from Beijing Vital River Laboratory Animal Technology Co., Ltd. GLP-1R knockout mice (GLP-1R$^{-/-}$) were purchased from Beijing Biocytogen Co., Ltd, and their identification was shown in Fig. S6. All animals were kept in SPF conditions with a constant ambient temperature of 25 °C, a constant humidity of 55 % and a 12-h light-dark cycle. All animals were free for water and food. All procedures on experimental animals were approved by the Animal Care and Use Committee of Tongji Medical College, Huazhong University of Science and Technology. (Ethics No.: TJH-202403008)

2.2. Cells

Hep-G2 cells were generously provided by Taize Biotechnology Co., Ltd. (Guangzhou, China). The cells were cultured in MEM medium (BioChannel, Nanjing, China) with 10 % FBS in a cell incubator with a constant ambient temperature of 37 °C and a stable gas composition of 5 % CO2 and 95 % air.

2.3. Reagents

Liraglutide (Novo Nordisk) was dissolved in normal saline and administered subcutaneously to mice at a dose of 200 μg/kg. GLP-1 (9–37) (NJPeptide, Nanjing, China), ferrostatin-1 (SML0583, Sigma-Aldrich), ML385 (CM05324, Proteintech, Wuhan, China) and LDN193189 (T1935, TargetMol, USA) were dissolved in DMSO for storage and then diluted in normal saline at the time of administration. GLP-1(9–37) (200 μg/kg) was administered subcutaneously to mice. Ferrostatin-1 (10 mg/kg), ML385 (30 mg/kg) and LDN193189 (3 mg/kg) were administered intraperitoneally to mice. A 2 % carbonyl iron food (high iron diet) was purchased from Beijing Vital River Laboratory Animal Technology Co., Ltd.

2.4. Hepatic ischemia-reperfusion model

Male C57BL/6 mice aged six to eight weeks were utilized as the experimental animals. The HIRI model was established as previously described [30]. The experimental mice were fully anesthetized with 1 % sodium pentobarbital, and the abdominal surgical area was shaved and sterilized with 75 % ethanol. The abdominal cavity was accessed through an incision along the abdominal midline, and the hepatic artery and portal vein supplying the left and middle lobes were clamped with a microvascular clip, resulting in the ischemia in 70 % of the liver lobes (the liver lobe changed from bright red to earth yellow). After 60 min of ischemia, the clip was removed and the abdominal cavity was closed with silk sutures. The postoperative mice were placed in an animal incubator at 32 °C until consciousness. Mice were sacrificed for sampling when the reperfusion time reached 6 h. The mice in the sham operation group underwent the same surgical procedure as the model group, except the portal vein and hepatic artery were not clamped.

2.5. Cell hypoxia and reoxygenation model

Hep-G2 cells were seeded in 6-well or 12-well plates. When the cell density reached approximately 70%–80 %, the cells were starved in serum-free MEM medium for 12 h to synchronize the cell state, and then placed in a H35 hypoxic workstation (Don whitley scientific, UK) with conditions of 1 % O_2, 5 % CO_2 and 94 % N_2. After 48 h of hypoxia, the cells were reoxygenated under normoxia conditions, and the medium was replaced with complete MEM medium containing PBS, Lira, GLP-1 (9–37) or Fer-1. Following 6 h of reoxygenation, the cells were collected for subsequent assays.

2.6. Measurement of ALT, AST, and LDH

The serum levels of ALT and AST, as well as the LDH levels in the cell culture supernatant, were quantified by an automatic biochemical analyzer (BS-200, Mindray).

2.7. H&E staining

Liver tissue samples of appropriate size were cut, fixed in 4 % paraformaldehyde and embedded in paraffin. Subsequently, the tissues were finely sectioned at a thickness of 5 μm. These sections underwent staining with hematoxylin and eosin dyes before scrutiny under a microscope. The evaluation of mouse liver injury was conducted using Suzuki's liver pathological score [31]. The scoring criteria were as follows: 0, no necrotic area; 1, single cell necrosis; 2, necrosis area <30 %; 3, necrosis area was 31–60 %; 4, the necrotic area >60 %.

2.8. TUNEL staining

TUNEL staining of liver paraffin sections was performed following the manufacturer's instructions for the TUNEL assay kit (A113-01, Vazyme Biotech Co.,Ltd, Nanjing, China).

2.9. Measurement of ROS in liver tissues and cells

The DHE probe (D7008-10, Sigma-Aldrich) was employed to assess the ROS levels in liver frozen sections and the DCFH-DA probe (S0033S, Beyotime Institute of Biotechnology) was utilized to determine the intracellular ROS levels in Hep-G2 cells, following the guidelines provided by the respective manufacturers.

The mitochondrial ROS in Hep-G2 cells was detected with the MitoSOX Red Kit (S0061S, Beyotime Institute of Biotechnology) in accordance with the manufacturer's guidelines.

2.10. Measurement of lipid peroxides, antioxidants and Fe^{2+} in liver tissue and Hep-G2 cells

Liver tissue and Hep-G2 cell homogenates were prepared, and the quantification of MDA, GSH, SOD and Fe^{2+} levels were conducted using assay kits according to the manufacturer's instructions. All the assay kits for MDA, GSH, SOD and Fe^{2+} were purchased from Elabscience Biotechnology Co.,Ltd (Wuhan, China).

The Fe^{2+} in Hep-G2 cells was also detected with FerroOrange probe (F374, DOJINDO, Japan) in accordance with the manufacturer's guidelines.

2.11. Immunohistochemistry

After being dewaxed, hydrated and subjected to antigen retrieval, the paraffin sections were blocked with 10 % goat serum. Subsequently, the sections were incubated with primary antibodies against GPX4 (1:200, A11243, ABclonal Technology), COX2 (1:400, 66351-1-Ig, Proteintech) and NRF2 (1:200, 16396-1-AP, Proteintech) overnight at 4 °C. Following this, the sections were incubated with an HRP-labeled secondary antibody at room temperature for 1 h. Finally, after DAB and hematoxylin staining, dehydration and sealing, the sections underwent microscopic examination.

2.12. Immunofluorescence

Hep-G2 cells were seeded on cell slides for immunofluorescence. After being fixed with 4 % paraformaldehyde and permeabilized with 0.5 % Triton-X-100, the cells were blocked with 10 % goat serum. Subsequently, the cells were incubated with primary antibodies against 4-HNE (1:200, Ab48506, Abcam), GPX4 (1:200, A11243, ABclonal Technology) and COX2 (1:200, 66351-1-Ig, Proteintech) overnight at 4 °C. Following this, the cells were treated with fluorescent secondary antibodies and underwent DAPI staining. Finally, the cells were visualized by a fluorescence microscopy.

2.13. Western blot

Proteins from liver tissues and Hep-G2 cells were extracted with RIPA lysate (P0013E, Beyotime Institute of Biotechnology, Shanghai, China), and the cytoplasmic and nuclear proteins were extracted with Nuclear and Cytoplasmic Protein Extraction Kit (KTP3001, Abbkine, Wuhan, China). Subsequently, tissue proteins (80 μg) and cell proteins (40 μg) were separated through electrophoresis and transferred to PVDF membranes. The blots were blocked with 5 % skim milk and then incubated overnight at 4 °C with primary antibodies against GPX4 (1:2000, A11243, ABclonal), COX2 (1:1000, 66351-1-Ig, Proteintech), NOX4 (1:1000, A22149, ABclonal), 4-HNE (1:1000, Ab48506, Abcam), Nrf2 (1:2000, A21508, ABclonal), NQO1 (1:2000, A22290, ABclonal), SOD (1:2000, A0274, ABclonal), HO-1 (1 : 1000, A19062, ABclonal), GSK3β (1:2000, A11731, ABclonal), p-GSK3β (1:2000, AP1088, ABclonal), FTH (1:2000, A19544, ABclonal), FTL (1:1000, 10727-1-AP, Proteintech), TfR1 (1:500, A21622, ABclonal), STAT3 (1:1000, #12640, Cell Signaling Technology), p-STAT3 (1:2000, #9145, Cell Signaling Technology), Hepcidin (1:1000, DF6492, Affinity Biosciences), SMAD159 (1:1000, ab300164, Abcam), SMAD4 (1:1000, #46535, Cell Signaling Technology), NCOA4 (1:500, DF4255, Affinity Biosciences), LC3 (1:1000, #12741, Cell Signaling Technology), P62 (1:500, A19700, ABclonal), IRP1 (1:1000, 12406-1-AP, Proteintech) and IRP2 (1:1000, 29976-1-AP, Proteintech). Upon incubation with HRP-labeled secondary antibodies, the blots were visualized with ECL solution. The gray-scale intensities of the blots were quantified by Image J.

2.14. qPCR

The RNA from liver tissues and Hep-G2 cells was isolated using an RNA extraction kit (220010, Fastagen, Shanghai, China). Subsequently, the extracted RNA underwent reverse transcription into cDNA utilizing a cDNA Synthesis SuperMix (11141 ES, YEASEN). Finally, the cDNA was quantitatively amplified with ChamQ SYBR qPCR Master Mix (High ROX Premixed) (Q341-02/03, Vazyme), and the mRNA levels were analyzed based on the CT values. The specific primer sequences are shown in Table S1.

2.15. Cell viability assay

The viability of Hep-G2 cells was assessed by a CCK8 assay kit (40203 ES, YEASEN) following the manufacturer's guidelines.

2.16. Transmission electron microscope (TEM)

Fresh mouse liver tissues were rapidly cut into 1 mm^3 cubes and thoroughly immersed in electron microscope fixative. After fixation, dehydration, and embedding, the samples were sectioned into 70 nm-sized slices. Subsequently, these sections were stained with 3 % uranyl acetate and lead citrate. Finally, the mitochondrial structure within the sections were visualized by utilizing a transmission electron microscope.

2.17. Assessment of mitochondrial membrane potential

The JC-1 fluorescent probe (C2005, Beyotime Institute of Biotechnology) was utilized to assess the mitochondrial membrane potential in Hep-G2 cells following the guidelines provided by the manufacturer.

2.18. RNA IP

The RNA Immunoprecipitation (RIP) assay was conducted utilizing the RIP kit (Bes5101, Guangzhou Bersinbio Bioscience CO., LTD, China) following the instructions provided by the manufacturer. Briefly, the *anti*-IRP1 antibody (12406-1-AP, Proteintech) was added to the cell lysate to immunoprecipitate IRP1. Subsequently, the RNA bound to IRP1 was isolated and quantified by qPCR. The rabbit IgG was utilized as the

negative control.

2.19. Statistical analysis

In this study, quantitative data were presented as Mean ± SEM. The differences between the two groups were analyzed using an Independent-Sample T Test, with a P-value below 0.05 deemed as statistically significant. All data analysis and statistical charts were produced with GraphPadPrism 8.

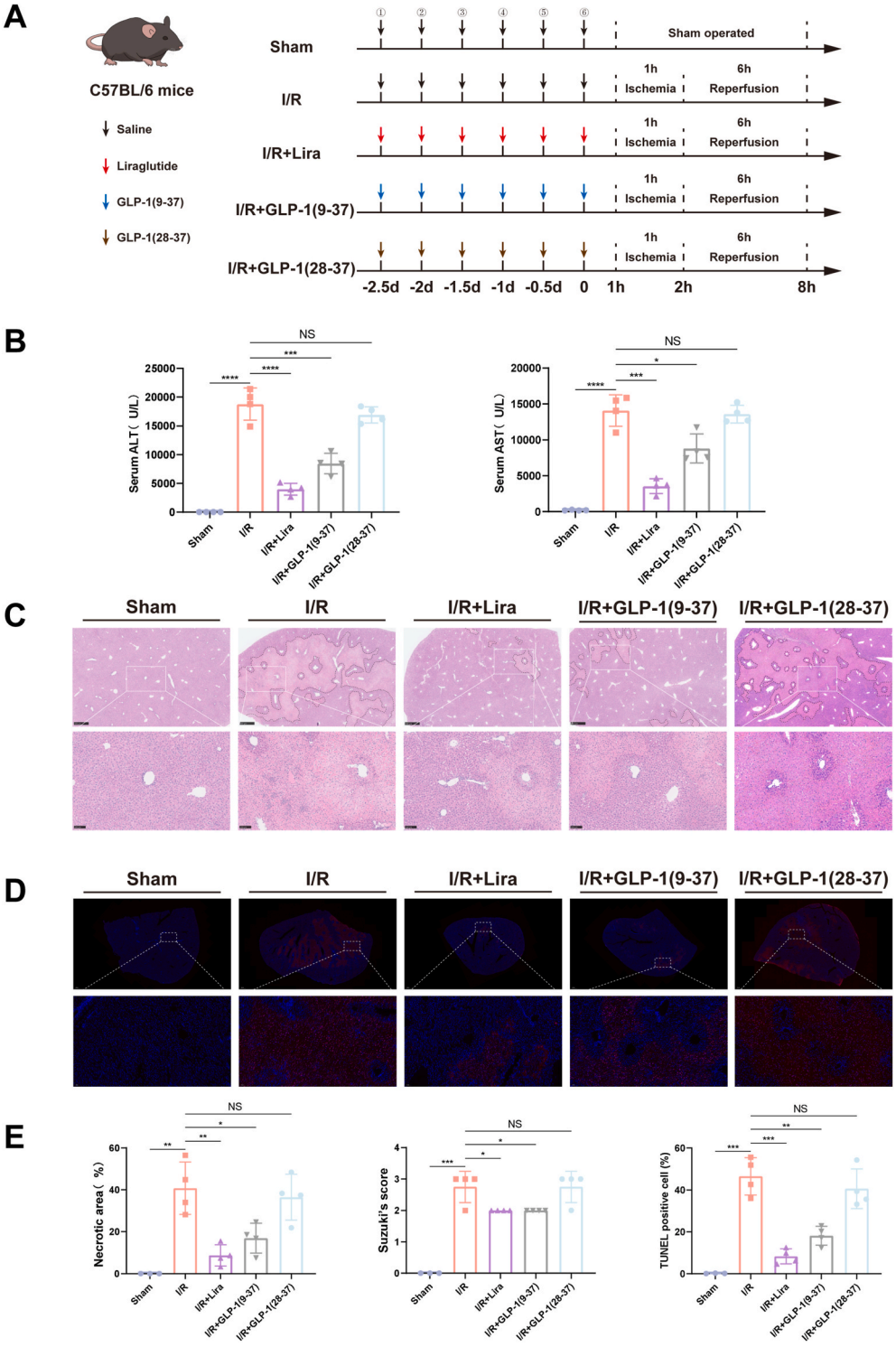

Fig. 1. Liraglutide and GLP-1(9–37) attenuated hepatic ischemia-reperfusion injury in vivo.
(A) Detailed treatment in vivo. Black arrows refer to saline, red arrows refer to liraglutide (200 μg/kg), blue arrows refer to GLP-1(9–37) (200 μg/kg) and brown arrows refer to GLP-1(28–37) (200 μg/kg). (B) The ALT and AST levels in mice with different treatment (n = 4). The liver injury was showed by the representative H&E staining (C) and the representative TUNEL staining (D). And the size of necrotic area, the Suzuki's score and the proportion of TUNEL positive cells were shown (E). Data were presented by the mean ± SEM. *P<0.05; **P<0.01; ***P<0.001; ****P<0.0001; NS refers to non-significant.

3. Results

3.1. Liraglutide (Lira) and its metabolite GLP-1(9–37) attenuated the liver injury induced by ischemia-reperfusion (I/R) in mice

First of all, we assessed the drug toxicity of Lira and its metabolites. The results showed that they did not cause any significant pathological changes in major organs, including the intestine, lung, kidney, heart, and liver, during the treatment period (Fig. S1A). Besides, they also did not result in significant changes in injury markers, including ALT, AST, CK, CREA, UREA, and LDH (Fig. S1B). In terms of body weight, Lira treatment resulted in a significant weight loss in mice, whereas its metabolites did not have this effect (Fig. S1C). Subsequently, we explored the optimal modeling condition. We assessed the liver injury in mice at 1, 3, 6, 12, 24 h of reperfusion after 1 h ischemia, respectively. Both pathological examination and liver injury markers indicated that the liver damage was most severe at 6 h of reperfusion (Figs. S2A and S2B). Therefore, we chose the time point of 1-h ischemia and 6-h reperfusion for our modeling condition.

To investigate the protective effect of Lira and its metabolites on HIRI

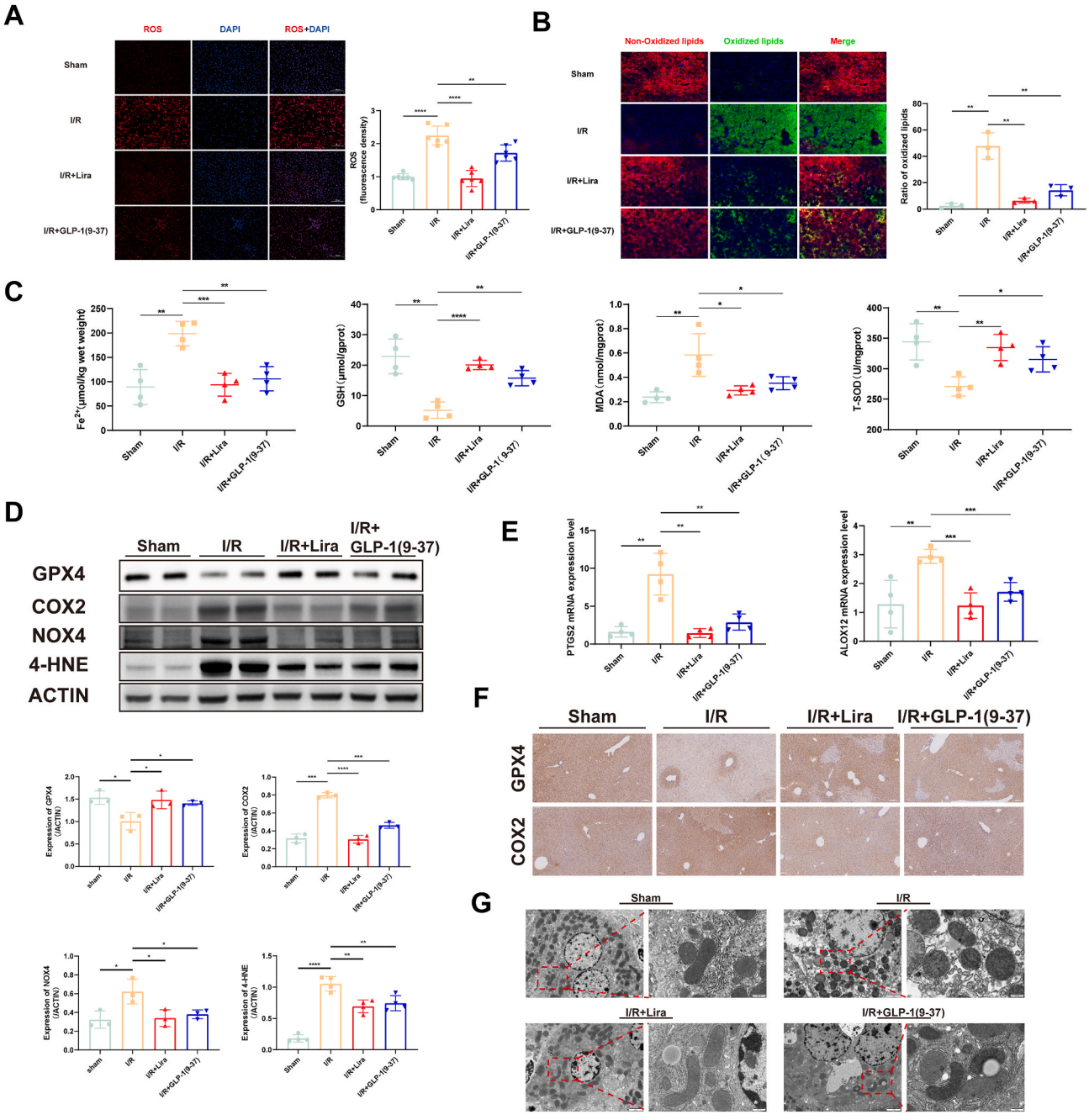

Fig. 2. Liraglutide and GLP-1(9–37) alleviated the ferroptosis following hepatic I/R injury.
(A) The level of ROS production in liver tissues was performed by DHE fluorescence probe, and the fluorescence density of ROS was calculated (n = 6). (B) The lipid peroxidation level in liver tissues was measured by C11-BODIPY probe (200 ×) and the ratio of oxidized lipids was shown (n = 3). (C) The content of MDA, GSH, Fe^{2+} and the activity of T-SOD in each group (n = 4–5). (D) The protein expression of GPX4, COX2, NOX4 and 4-HNE in liver tissues was measured by Western blot, and quantitative analysis of the results was performed (n = 3). (E) The mRNA levels of PTGS2 and ALOX12 in liver tissues (n = 4). (F) Representative images of the immunohistochemical staining of GPX4 and COX2 in liver tissues. (G) Representative TEM images of liver tissues in each group. Data were presented by the mean ± SEM. *P<0.05; **P<0.01; ***P<0.001; ****P<0.0001.

in mice, we randomly divided the mice into five groups, and the specific grouping and dosing regimens were shown in Fig. 1A (Fig. 1A). Biochemical results showed that compared with the Sham group, hepatic ischemia-reperfusion significantly increased the levels of ALT and AST in the serum of mice, which was significantly reversed by Lira and GLP-1(9–37) preconditioning (Fig. 1B). H&E staining results showed that I/R caused extensive hepatocyte necrosis (with necrotic areas exceeding 40 %), hyperemia and substantial inflammatory cell infiltration in the injured areas, while preconditioning with Lira and GLP-1(9–37) significantly reduced the tissue damage induced by I/R (Fig. 1C–E). In line with the HE results, TUNEL staining of liver tissue showed a marked increase in apoptotic positive cells in the I/R group, while preconditioning with Lira and GLP-1(9–37) significantly decreased the number of apoptotic cells (Fig. 1D and E). However, the above protective effects were not observed in the GLP-1(28–37) treatment group (Fig. 1B, C, D, E). These results indicated that both Lira and

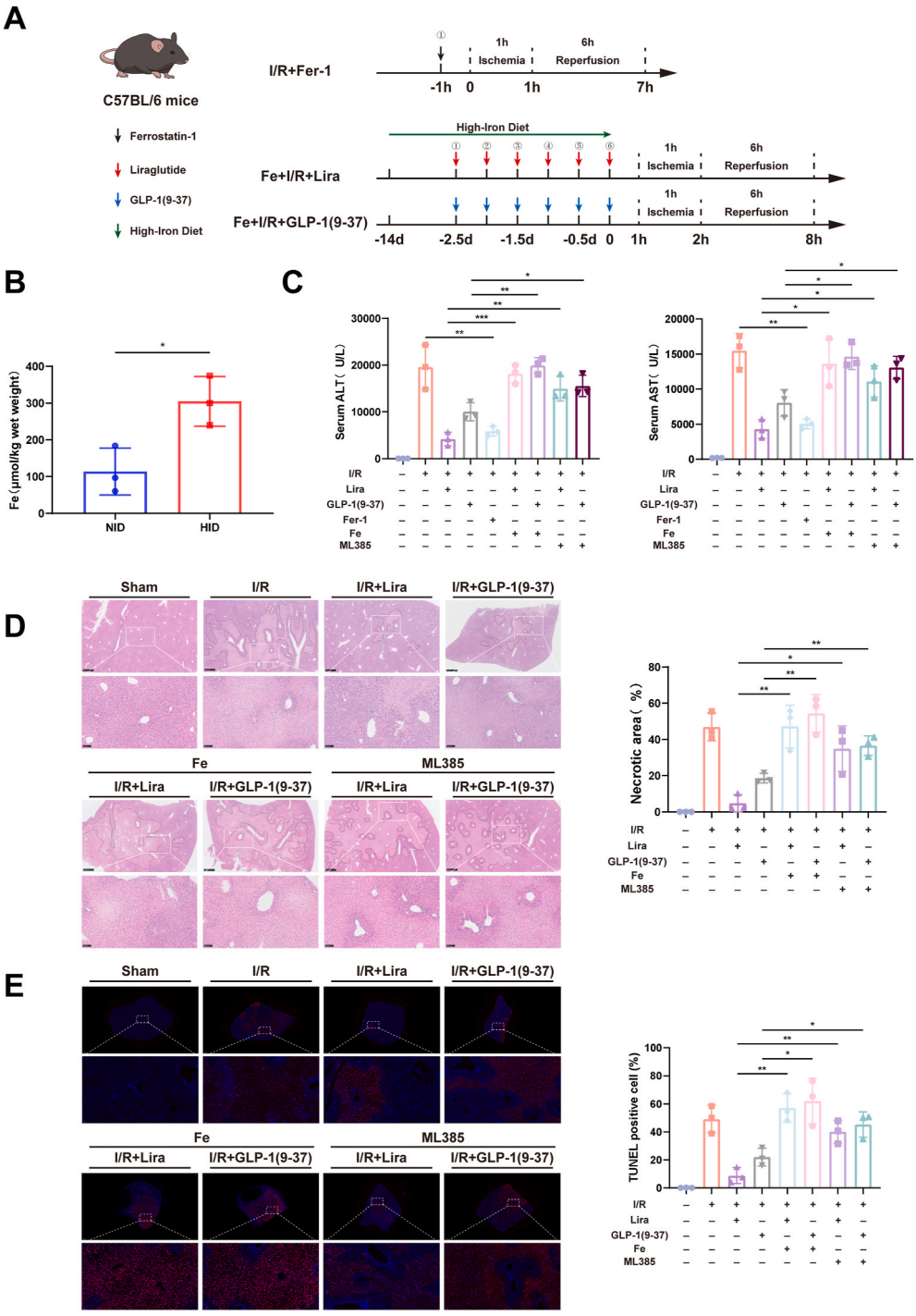

Fig. 3. The protective effects of Lira and GLP-1(9–37) on hepatic ischemia-reperfusion injury were related to their inhibitory effects on ferroptosis.
(A) Detailed treatment in vivo. Black arrows refer to ferrostatin-1, red arrows refer to liraglutide (200 μg/kg), blue arrows refer to GLP-1(9–37) (200 μg/kg) and green arrows refer to High-Iron diet (2 % carbonyl iron diet). (B) The determination of total iron content in liver tissues (n = 3). (C) The ALT and AST levels in mice with different treatment (n = 3). (D) The representative H&E staining of liver tissues and the size of necrotic area (n = 3). (E) The representative of TUNEL staining of liver tissues and the proportion of apoptosis positive cells (n = 3). Data were presented by the mean ± SEM. *P<0.05; **P<0.01; ***P<0.001.

GLP-1(9–37) could attenuate HIRI in mice, while GLP-1(28–37) did not have this effect. Thus, we only investigated the effects of Lira and GLP-1 (9–37) in the subsequent experiments.

3.2. Lira and GLP-1(9–37) attenuated the ferroptosis triggered by hepatic ischemia-reperfusion

Firstly, we determined whether ferroptosis occurs in the HIRI model used in this study. We assessed the levels of oxidized lipids as well as the expression of GPX4 and PTGS2. The results showed that at the time point of 6-h reperfusion, in addition to the most severe damage, there were also the highest level of oxidized lipids, the lowest expression of GPX4, and the highest expression of PTGS2 (Figs. S2C, S2D, S2E). Besides, ferrostatin-1 (Fer-1), a ferroptosis inhibitor, was administered to mice as illustrated in Fig. 3A (Fig. 3A), and the protective effect of Fer-1 on HIRI was evaluated by measuring the liver enzyme levels. The results showed that an intraperitoneal injection of 10 mg/kg Fer-1, administered 1 h before surgery, significantly decreased serum ALT and AST levels, which indicated the protective effect of Fer-1 on HIRI and confirmed the involvement of ferroptosis in the HIRI model we used (Fig. 3C).

Next, we evaluated the effects of Lira and GLP-1(9–37) on the ferroptosis in HIRI by examining multiple ferroptosis-related indicators. The ROS level in liver tissues was detected with the DHE probe. It was found that the ROS level significantly increased after I/R, while preconditioning with Lira and GLP-1(9–37) significantly reduced the I/R-induced ROS increase (Fig. 2A). The oxidized lipids, Fe^{2+}, MDA, GSH and SOD levels in liver tissues were also measured. The results showed that I/R increased the levels of oxidized lipids, Fe^{2+} and MDA, and decreased the levels of GSH and SOD in liver tissues, while preconditioning with Lira and GLP-1(9–37) significantly reduced the oxidized lipids, Fe^{2+} and MDA levels and increased GSH and SOD levels in liver tissues (Fig. 2B and C). What's more, the levels of several ferroptosis-related proteins were detected. The results showed a substantial reduction in the expression of GPX4 following I/R, while Lira and GLP-1(9–37) preconditioning increased its expression. Conversely, the expressions of COX2, NOX4, and 4-HNE were significantly increased after I/R, and their levels were reduced by preconditioning with Lira and GLP-1(9–37) (Fig. 2D). The immunohistochemical results of GPX4 and COX2 in liver tissues were consistent with the Western blot findings (Fig. 2F). At the mRNA level, PTGS2 and ALOX12, associated with ferroptosis, were significantly upregulated by I/R, while these increases were blocked by Lira and GLP-1(9–37) preconditioning (Fig. 2E). Finally, we observed the mitochondrial morphology in liver tissues and found that I/R caused significant mitochondrial destruction, evidenced by heightened density, shortened long diameter, and decreased mitochondrial cristae, which was significantly attenuated by Lira and GLP-1 (9–37) preconditioning (Fig. 2G). These results suggested that Lira and GLP-1(9–37) could reduce the levels of free iron and lipid peroxides, alleviate the oxidative damage in the liver tissues after I/R, and thereby inhibit the occurrence of ferroptosis.

3.3. Lira and GLP-1(9–37) exert protective effects against HIRI by attenuating ferroptosis

To investigate whether the protective effects of Lira and GLP-1(9–37) on HIRI were related to their effects on inhibiting ferroptosis, we fed mice with a high-iron diet (HID) containing 2 % carbonyl iron, which was used to exacerbate the ferroptosis during I/R by increasing liver iron content [11]. Subsequently, we observed whether the protective effects of Lira and GLP-1(9–37) were affected under this condition. The detailed experimental protocol was shown in Fig. 3A (Fig. 3A). After 14 days of HID feeding, the total iron level in mouse liver tissues showed a significant increase (Fig. 3B). Biochemical analysis showed that HID feeding significantly attenuated the effects of Lira and GLP-1(9–37) on reducing the ALT and AST levels in the serum of postoperative mice (Fig. 3C). H&E pathological staining results also revealed significantly worse liver injury, larger necrotic areas, and more inflammatory cell infiltration in the Lira and GLP-1(9–37) preconditioning groups after HID feeding (Fig. 3D). Furthermore, TUNEL staining of liver tissues demonstrated that HID feeding resulted in a marked increase in the percentage of apoptotic positive cells in the Lira and GLP-1(9–37) preconditioning groups, aligning with the findings from HE staining (Fig. 3E). These results indicated that HID feeding markedly attenuated the protective effects of Lira and GLP-1(9–37) on HIRI, indicating a correlation between the inhibitory effects of Lira and GLP-1(9–37) on ferroptosis and their efficacy in protecting against HIRI.

3.4. Lira and GLP-1(9–37) could inhibit the ferroptosis in hepatic ischemia-reperfusion through a GLP-1R-independent pathway

Previous studies have found that GLP-1R agonists and metabolites still have partial effects in GLP-1R knockout (GLP-$1R^{-/-}$) mice [24,25,32]. Thus, we explored whether the inhibitory effects of Lira and GLP-1 (9–37) on the ferroptosis in HIRI were also not entirely dependent on GLP-1R. To investigate this, We used GLP-$1R^{-/-}$ mice as the experimental animals to establish the HIRI model, following the same procedure as with WT mice. The detection of ROS revealed that in GLP-$1R^{-/-}$ mice, Lira and GLP-1(9–37) still slightly decreased the ROS levels in the liver after I/R (Fig. 4A). Additionally, the analysis of oxidized lipids, Fe^{2+}, SOD, GSH and MDA levels in liver tissues showed that in the absence of GLP-1R, Lira and GLP-1(9–37) preconditioning still reduced the oxidized lipids, Fe^{2+} and MDA levels and elevated GSH levels, with no change in SOD levels (Fig. 4B and C). Furthermore, the expression of ferroptosis-related proteins was also examined. It was found that preconditioning with Lira and GLP-1(9–37) still increased the expression of GPX4 in the liver of GLP-$1R^{-/-}$ mice, and suppressed the expression of 4-HNE and COX2 (Fig. 4D). These results suggested that there might be a GLP-1R-independent pathway for the inhibitory effects of Lira and GLP-1(9–37) on the ferroptosis in HIRI.

3.5. Lira and GLP-1(9–37) attenuated the cell damage induced by hypoxia-reoxygenation (H/R) in Hep-G2 cells

Previous research has elucidated that ferroptosis predominantly occurs in hepatocytes during hepatic ischemia-reperfusion [13]. Thus, we further investigated whether Lira and GLP-1(9–37) inhibited the ferroptosis in hepatocytes during HIRI. In the in vitro study, a cellular hypoxia-reoxygenation model was utilized to simulate the ischemia-reperfusion injury in vivo, and Hep-G2 cells were utilized as a model for human hepatocytes. After exploration, we finally determined the experimental regimen of H/R as 48 h of hypoxia followed by 6 h of reoxygenation. The specific experimental regimen and drug treatment details were shown in Fig. 5A (Fig. 5A). Initially, multiple drug concentration gradients of Lira and GLP-1(9–37) were tested to determine their protective effects and appropriate dose. The results of the CCK-8 assay revealed a substantial reduction in the viability of Hep-G2 cells following H/R, which was only about half of that of the Control group. However, as the drug concentration increased, both Lira and GLP-1 (9–37) demonstrated protective effects against H/R-induced cell damage in Hep-G2 cells. The optimal and stable protective effects were observed at a concentration of 25 μmol/L for both Lira and GLP-1(9–37) (Fig. 5B). Consequently, 25 μmol/L was chosen as the concentration for both Lira and GLP-1(9–37) in the subsequent cell experiments. Then, the content of LDH in the cell culture supernatant was measured. It was found that H/R caused a significant increase in LDH levels in the supernatant, while both Lira and GLP-1(9–37) treatment at 25 μmol/L reduced the H/R-induced increase in LDH levels (Fig. 5C). These results demonstrated that both Lira and GLP-1(9–37) provided protective effects against the cell damage induced by H/R in Hep-G2 cells.

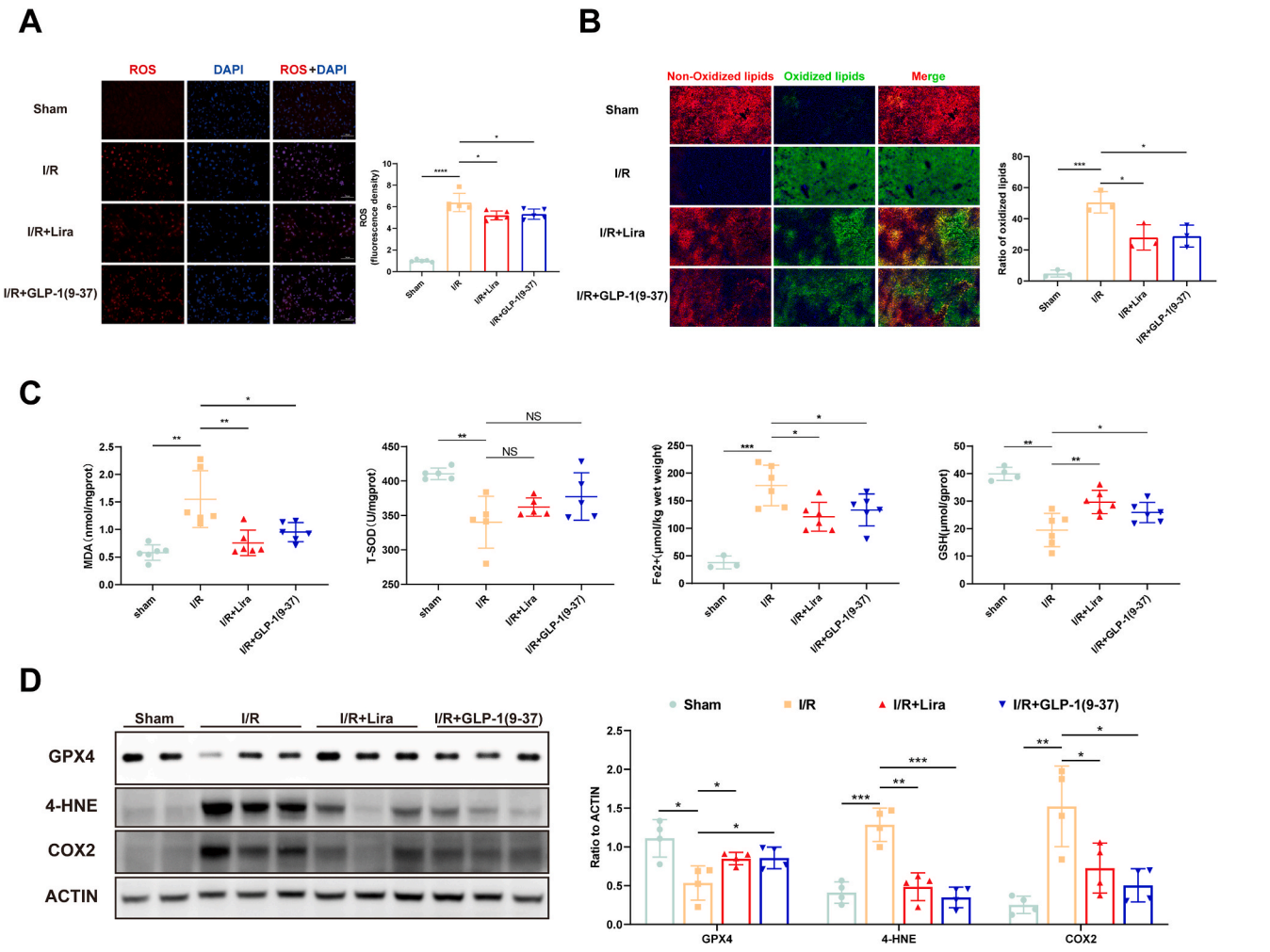

Fig. 4. Liraglutide and GLP-1(9–37) also alleviated the ferroptosis in GLP-1R$^{-/-}$ mice following hepatic I/R injury.
(A) The assessment of ROS levels in liver tissues of GLP-1R$^{-/-}$ mice was performed by DHE fluorescence probe, and the fluorescence density of ROS was calculated (n = 5). (B) The lipid peroxidation level in liver tissues of GLP-1R$^{-/-}$ mice was detected by C11-BODIPY probe (200 ×) and the ratio of oxidized lipids was shown (n = 3). (C) The content of MDA, GSH, Fe^{2+} and the activity of T-SOD in liver tissues of GLP-1R$^{-/-}$ mice in each group (n = 3–6). (D) The protein expression of GPX4, COX2 and 4-HNE in liver tissues of GLP-1R$^{-/-}$ mice was measured by Western blot, and the quantitative results were performed (n = 4). Data were presented by the mean ± SEM. *P<0.05; **P<0.01; ***P<0.001; ****P<0.0001; NS refers to non-significant.

3.6. Lira and GLP-1(9–37) attenuated the ferroptosis triggered by H/R in Hep-G2 cells

In the in vivo study, we verified that Lira and GLP-1(9–37) preconditioning could attenuate the ferroptosis triggered by hepatic ischemia-reperfusion. In the in vitro study, we further investigated whether Lira and GLP-1(9–37) could also mitigate the ferroptosis triggered by H/R in Hep-G2 cells. First, to confirm the presence of ferroptosis in the H/R model of Hep-G2 cells, Fer-1 was utilized following the experimental regimen depicted in Fig. 5A (Fig. 5A). The results of the CCK-8 assay showed that 3 μmol/L Fer-1 exerted a protective effect against H/R injury in Hep-G2 cells (Fig. 5B), which suggested the occurrence of ferroptosis in the H/R model of Hep-G2 cells.

Next, we measured the levels of lipid peroxides, free iron, and ferroptosis-related protein expressions in the cells from each group. The intracellular ROS levels were assessed by the DCFH-DA probe. Both flow cytometry detection and immunofluorescence images revealed that H/R significantly increased ROS levels in Hep-G2 cells, while both Lira and GLP-1(9–37) treatment reduced intracellular ROS levels after H/R (Fig. 6A, Fig. S3A). The mitochondrial ROS was observed by the MitoSOX probe, and the results showed that Lira and GLP-1(9–37) significantly blocked the increase of mitochondrial ROS induced by H/R (Fig. 6I). Meanwhile, H/R also resulted in an increase in the oxidized lipids and MDA and a decrease in the antioxidants GSH and SOD in Hep-G2 cells, while these effects were reversed by treatment with Lira and GLP-1(9–37) (Fig. 6B and C). The detection of intracellular Fe^{2+} content showed that H/R induced the accumulation of Fe^{2+} in Hep-G2 cells, which was mitigated by Lira and GLP-1(9–37) treatment (Fig. 6C). Correspondingly, the FerroOrange probe staining showed the same result that the fluorescence intensity of Hep-G2 cells was enhanced by H/R and weakened by Lira and GLP-1(9–37) treatment (Fig. 6D). At the protein expression levels, H/R induced a notable reduction in GPX4 levels and an elevation in COX2 levels in Hep-G2 cells, while these changes were reversed by Lira and GLP-1(9–37) treatment (Fig. 6E). And the corresponding fluorescence images showed the same result (Figs. S3B and S3C). At the mRNA level, H/R also induced an increase in PTGS2 and ALOX15, and these increases were markedly reduced by Lira and GLP-1(9–37) treatment (Fig. 6F). In addition, the immunofluorescence assay demonstrated that Lira and GLP-1(9–37) treatment significantly decreased the H/R-induced increase in 4-HNE content in Hep-G2 cells (Fig. 6G). Finally, mitochondrial membrane potential (MMP) was measured to evaluate the status of intracellular mitochondria. The results showed that the Control group exhibited predominantly red fluorescence, whereas H/R treatment resulted in a marked reduction in red

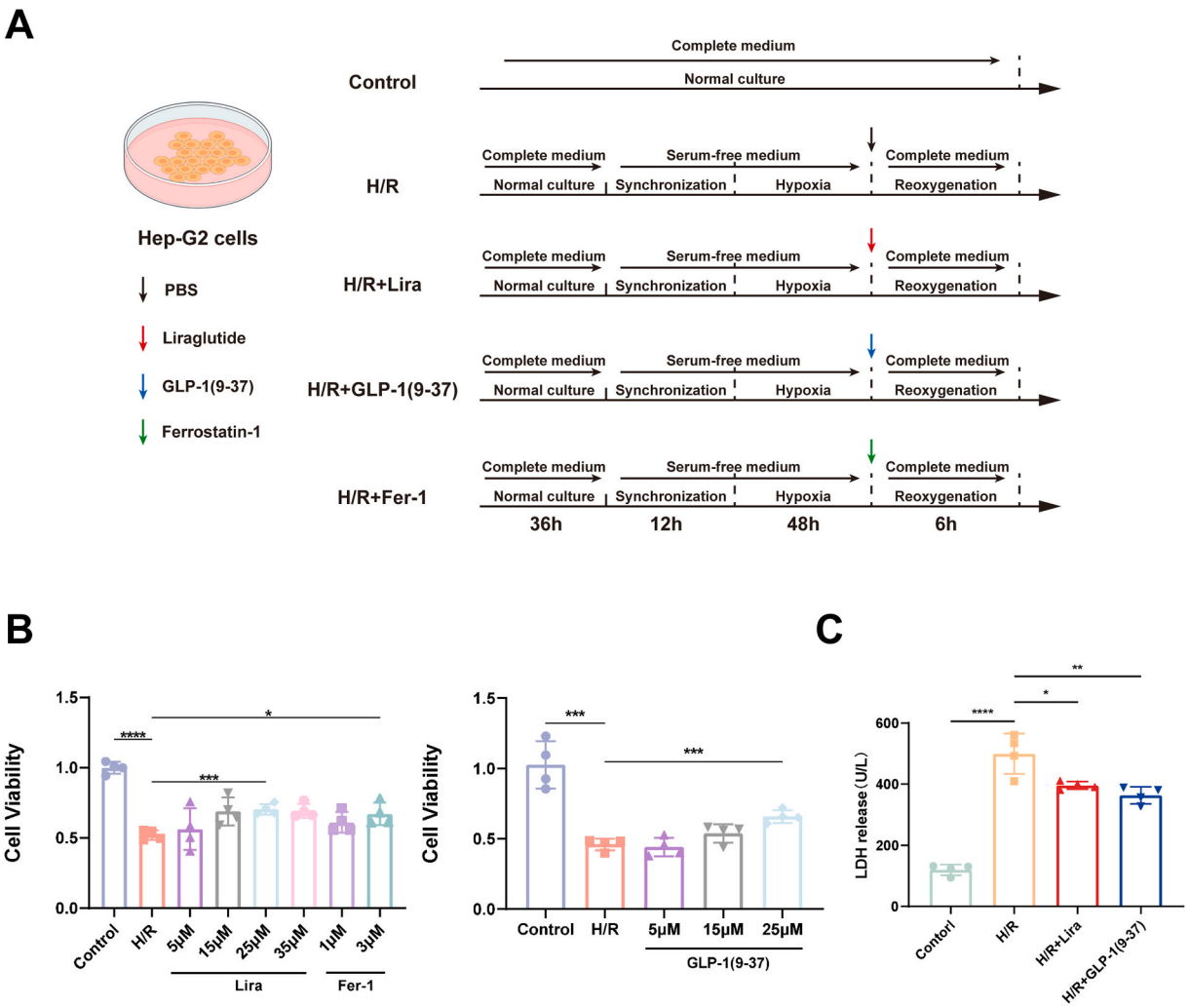

Fig. 5. Liraglutide and GLP-1(9–37) reduced the injury of Hep-G2 cells induced by hypoxia-reoxygenation.
(A) Detailed treatment in vitro. Black arrows refer to PBS, red arrows refer to liraglutide, blue arrows refer to GLP-1(9–37) and green arrows refer to ferrostatin-1. (B) The cell viability assessed by CCK-8 kit in different groups (n = 4). (C) The LDH levels in cell culture supernatant (n = 4). Data were presented by the mean ± SEM. *P<0.05; **P<0.01; ***P<0.001; ****P<0.0001.

fluorescence and an elevation in green fluorescence, indicating a decline in MMP and impaired mitochondrial function, which was reversed by Lira and GLP-1(9–37) treatment (Fig. 6H). These findings demonstrated that Lira and GLP-1(9–37) could reduce intracellular Fe^{2+} and lipid peroxides levels while enhancing the antioxidant capacity of Hep-G2 cells following H/R, thereby inhibiting the occurrence of ferroptosis.

3.7. Lira and GLP-1(9–37) reduced the lipid oxidation level by promoting the nuclear translocation of Nrf2 during hepatic ischemia-reperfusion and cell hypoxia-reoxygenation

To investigate how Lira and GLP-1(9–37) affect the ferroptosis in HIRI, we performed RNA sequencing on the livers of mice subjected to I/R, I/R + Lira, and I/R + GLP-1(9–37) treatments, respectively. Gene Ontology (GO) analysis on the differentially expressed genes between I/R and I/R + Lira groups showed that iron ion binding function and oxidoreductase function were enriched in the top 20 terms (Fig. S4A). Similarly, the same functions were also enriched in the GO analysis between I/R and I/R + GLP-1(9–37) groups (Fig. S4A). Given that ferroptosis is characterized by massive iron accumulation and lipid peroxidation, culminating in severe oxidative damage, we hypothesized that Lira and GLP-1(9–37) might inhibit ferroptosis through their ability to regulate iron metabolism and lipid peroxidation. So we explored the mechanisms underlying their ferroptosis-inhibiting effects through these two aspects.

Firstly, based on the RNA sequencing results, we analyzed the gene expression of oxidoreductases. Heatmap indicated that the gene expression of most oxidoreductases was significantly increased after the treatment with Lira or GLP-1(9–37) (Fig. S4B). Previous studies have established that most of these oxidoreductases were regulated by Nrf2, a key molecule for intracellular defense against oxidative stress [33]. Upon activation, it translocates to the nucleus, where it serves as a transcription factor, enhancing the expression of an array of antioxidant enzymes [33,34]. Thus, we next examined the activation of Nrf2. The total protein level of Nrf2 in liver tissues and Hep-G2 cells was detected, however, the results indicated that treatment with Lira and GLP-1(9–37) did not significantly change the total protein level of Nrf2 (Fig. 7A). Then, We further examined the nuclear translocation of Nrf2 in both the HIRI and H/R models. After I/R, the nuclear abundance of Nrf2 was increased, with no significant alteration in the cytoplasmic level, while preconditioning with Lira and GLP-1(9–37) further elevated the nuclear Nrf2 level and concomitantly reduced its cytoplasmic presence (Fig. 7B). The immunohistochemical assay corroborated these findings, showing an enhanced nuclear localization of Nrf2 following treatment with Lira and GLP-1(9–37) (Fig. 7C). Similar results were obtained in vitro, where treatment with Lira and GLP-1(9–37) significantly increased the nuclear

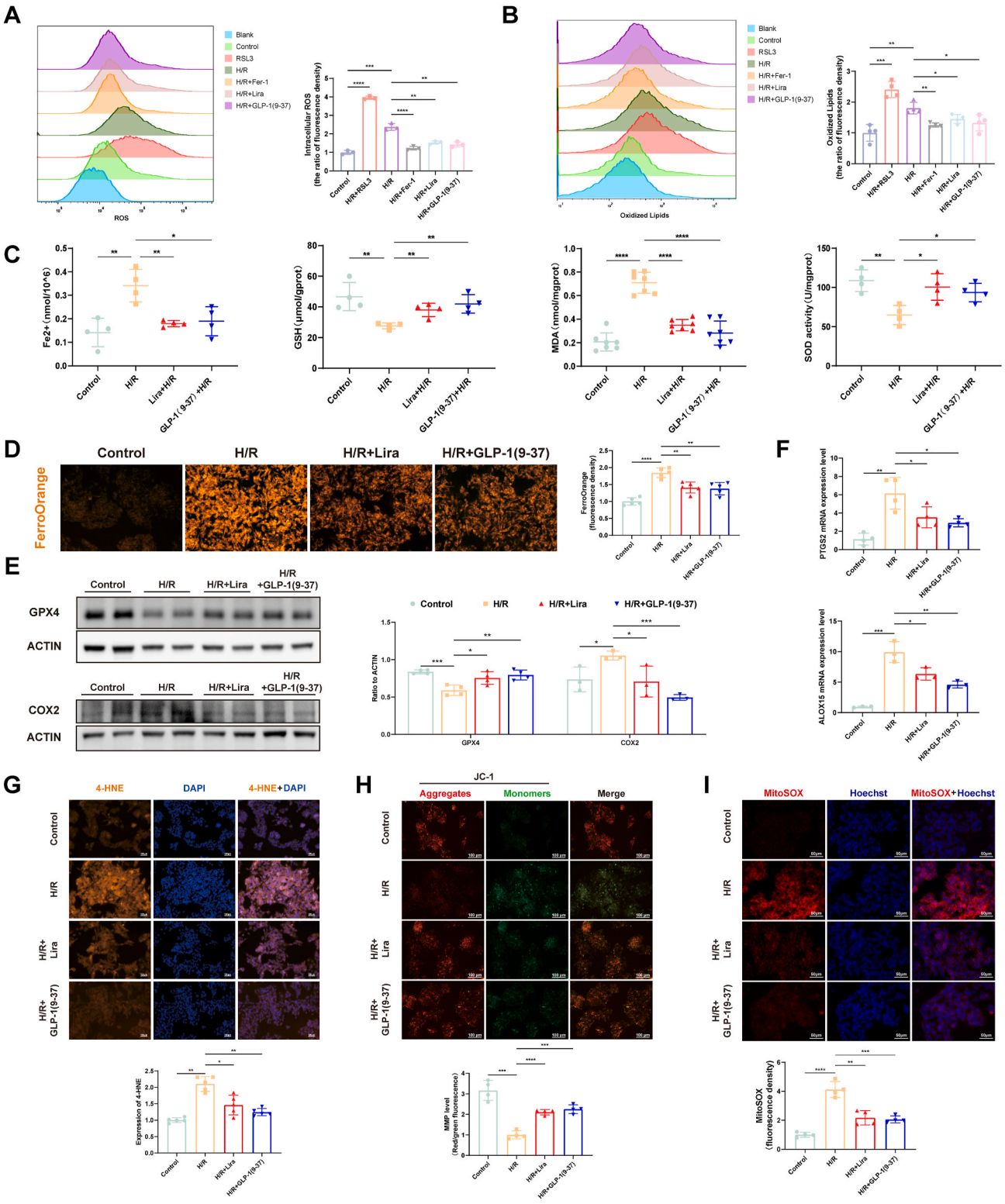

Fig. 6. Liraglutide and GLP-1(9–37) alleviated the ferroptosis induced by H/R in Hep-G2 cells.
(A) Intracellular ROS of each group was measured by flow cytometry and the quantification of ROS level was performed (n = 4). (B) The oxidized lipids in cells were detected by flow cytometry using C11-BODIPY probe and the ratio of fluorescence density was shown (n = 4). (C) The levels of Fe^{2+}, GSH, MDA and the activity of SOD in Hep-G2 cells with different treatment (n = 4–7). (D) The Fe^{2+} in cells was observed by FerroOrange probe and the fluorescence density was performed (n = 5). (E) The protein expression of GPX4 and COX2 in Hep-G2 cells was measured by Western blot, and the quantitative results were performed (n = 3–4). (F) The mRNA levels of PTGS2 and ALOX15 in Hep-G2 cells (n = 3–4). (G) The content of 4-HNE in Hep-G2 cells was measured by IF and the quantification was performed (n = 5). (H) MMP was measured by JC-1 probe and the level of MMP was performed as red/green fluorescence ratio (n = 4). (I) Mitochondrial ROS of each group was detected by MitoSOX Red Probe and the quantification was performed (n = 4). Data were presented by the mean ± SEM. *P<0.05; **P<0.01; ***P<0.001; ****P<0.0001.

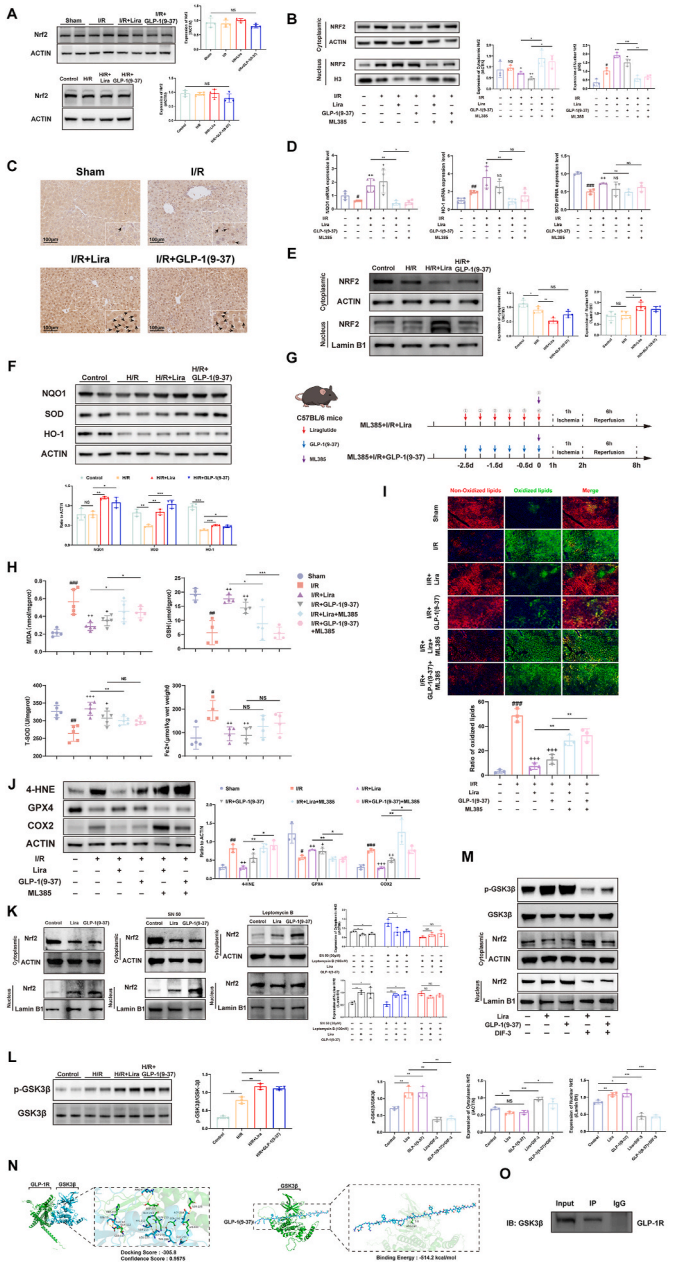

(caption on next column)

Fig. 7. Liraglutide and GLP-1(9–37) attenuated the level of lipid peroxidation by promoting NRF2 nuclear translocation both in vivo and in vitro.
(A) The total protein levels of Nrf2 in liver tissues and Hep-G2 cells were measured by WB, and the quantitative results were performed (n = 4). (B) The abundance of NRF2 in cytoplasm and nucleus in liver tissues was measured by Western blot and the quantitative result was performed (n = 3). (C) The nuclear translocation of NRF2 was observed by IHC (200 ×). (D) The mRNA levels of NQO1, HO-1 and SOD in liver tissues were assessed by quantitative real-time PCR (n = 3–4). (E) The NRF2 in the cytoplasm and nucleus in Hep-G2 cells was assessed by western bolt and the quantitative results were performed (n = 4). (F) The protein abundances of NQO1, SOD and HO-1 were assessed by Western blot and the quantification was performed (n = 3). (G) Detailed treatment in vivo. Red arrows refer to liraglutide (200 μg/kg), blue arrows refer to GLP-1(9–37) (200 μg/kg) and purple arrows refer to ML385 (30 mg/kg). (H) The levels of MDA, GSH, Fe^{2+} and the activity of T-SOD in each group (n = 4–5). (I) The lipid peroxidation level in liver tissues was detected by C11-BODIPY probe (200 ×) and the ratio of oxidized lipids was performed (n = 3). (J) The protein expression of GPX4, COX2 and 4-HNE in liver tissues was measured by Western blot and the quantification was performed (n = 3). (K) The abundance of NRF2 in cytoplasm and nucleus in Hep-G2 cells with SN50 (30 μM) or Leptomycin (100 nM) treatment was detected by WB, and the quantitative result was performed (n = 3). (L) The protein expression of GSK3β and *p*-GSK3β was assessed by Western blot and the quantification was performed (n = 3). (M) The levels of NRF2 in cytoplasm and nucleus after *p*-GSK3β inhibition by DIF-3 (10 μM) were measured by WB, and the quantitative result was performed (n = 3). (N) Molecular docking proposed the interaction mode of GLP-1R and GSK3β (Docking Score: −305.8; Confidence Score: 0.9575) and the interaction mode of GLP-1(9–37) and GSK3β (Binding Energy: −514.2 kcal/mol). (O) The interaction between GLP-1R and GSK3β was detected by immunoprecipitation. Data were presented by the mean ± SEM. $^{\#}P<0.05$, $^{\#\#}P<0.01$ $^{\#\#\#}P<0.001$ versus the Sham group; $^{+}P<0.05$, $^{++}P<0.01$, $^{+++}P<0.001$ versus the I/R group; *P<0.05; **P<0.01; ***P<0.001; NS refers to non-significant.

Nrf2 protein level in Hep-G2 cells (Fig. 7E). Meanwhile, we also examined the expression of Nrf2 downstream targets. In vivo, Lira preconditioning markedly elevated the mRNA levels of NQO1, HO-1, and SOD in liver tissues, whereas GLP-1(9–37) preconditioning increased the NQO1 mRNA level, without statistically significant effects on HO-1 and SOD (Fig. 7D). In vitro experiments demonstrated that both Lira and GLP-1(9–37) elevated the protein levels of NQO1, SOD, and HO-1 (Fig. 7F). These results suggested that both Lira and GLP-1(9–37) could facilitate the translocation of Nrf2 to the nucleus and induce the expression of its downstream antioxidant enzymes.

Then, to investigate whether the effects of Lira and GLP-1(9–37) on reducing lipid peroxides was related to the activation of Nrf2, we utilized an Nrf2-specific inhibitor, ML385, in vivo. The specific administration regimen was shown in Fig. 7G (Fig. 7G). We found that ML385 treatment significantly inhibited the nuclear translocation of Nrf2 promoted by Lira and GLP-1(9–37), resulting in an obvious reduction of Nrf2 in the nucleus coupled with an increase in the cytoplasm (Fig. 7B). Additionally, ML385 treatment also conspicuously decreased the mRNA levels of NQO1, HO-1, and SOD (Fig. 7D). These results indicated that the activity of Nrf2 were significantly inhibited by ML385 treatment. Biochemical assays, as well as HE and TUNEL staining, revealed that the inhibition of Nrf2 by ML385 significantly countered the protective effects of Lira and GLP-1(9–37), resulting in increased serum ALT and AST levels, enlarged areas of tissue necrosis and a higher proportion of apoptosis-positive cells (Fig. 3C, D, E). Furthermore, Nrf2 inhibition also countered the effects of Lira and GLP-1 (9–37) on oxidized lipids, SOD, GSH, and MDA levels, leading to an elevation in oxidized lipids and MDA levels and a reduction in GSH and SOD levels but no significant change in Fe^{2+} levels in liver tissues (Fig. 7H and I). What's more, following the inhibition of NRF2 in Lira and GLP-1(9–37) preconditioning group, the expression of 4-HNE and COX2 was highly increased, while the expression of GPX4 was significantly decreased (Fig. 7J). These findings indicated that Lira and GLP-1(9–37) reduced the lipid peroxidation level in HIRI by promoting Nrf2 nuclear translocation.

The nuclear abundance of Nrf2 is related to its nuclear import and export processes. Therefore, to investigate the reason why Lira and GLP-1(9–37) treatments increased the nuclear Nrf2 abundance, we utilized the nuclear import inhibitor SN50 and the nuclear export inhibitor Leptomycin B, respectively. The results showed that Lira and GLP-1 (9–37) treatments were still able to increase the nuclear Nrf2 abundance after nuclear import inhibition, while this effect was blocked after nuclear export inhibition (Fig. 7K). This finding indicated that Lira and GLP-1(9–37) might increase the nuclear abundance of Nrf2 by preventing its nuclear export. Previous studies have identified GSK3β as a

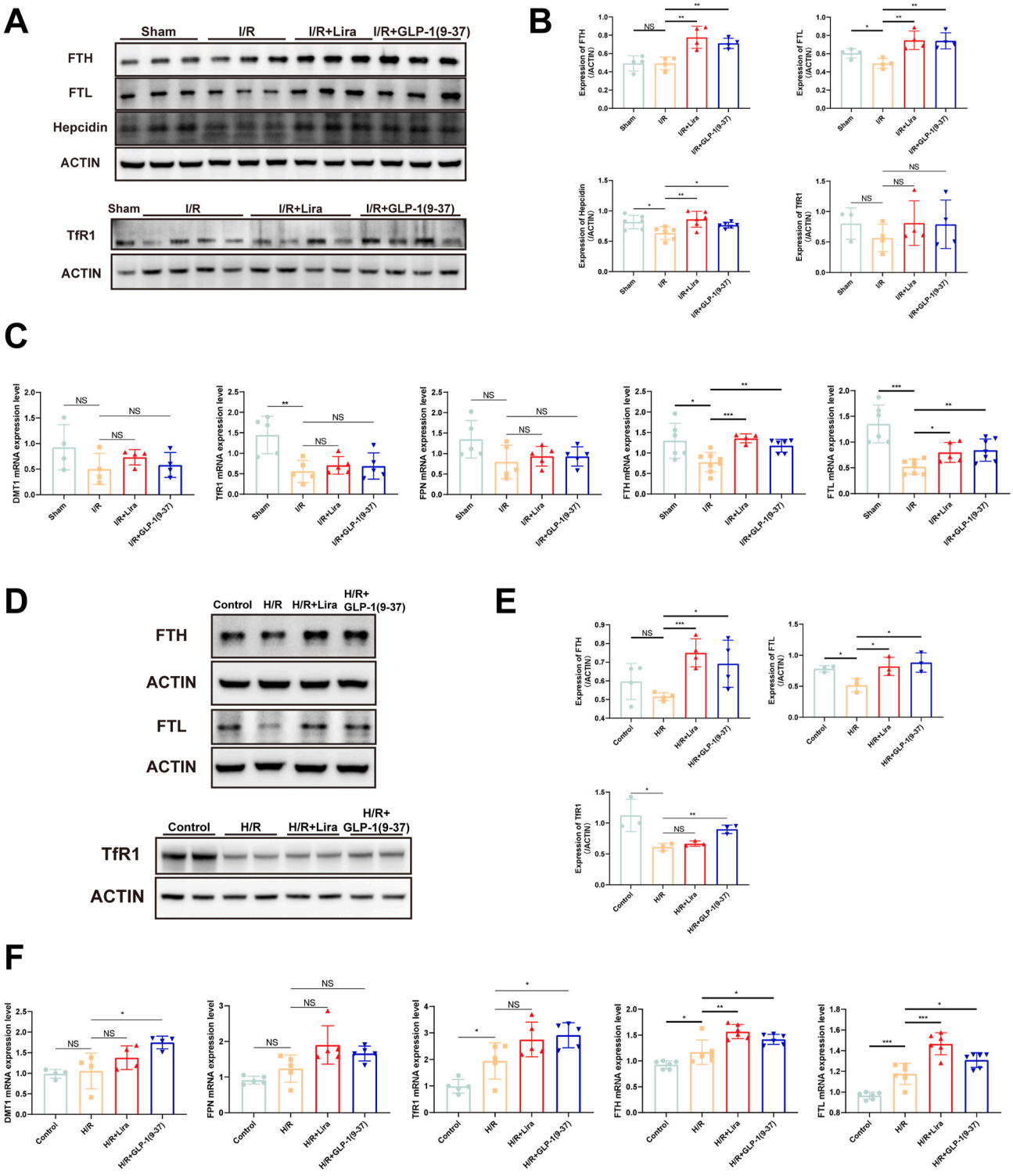

Fig. 8. Liraglutide and GLP-1(9–37) increased the expression of FTH and FTL in both in vivo and in vitro.
(A) The protein expression of FTH, FTL, Hepcidin and TfR1 in liver tissues. (B) The quantification of protein expression (n = 3–4). (C) The mRNA levels of DMT1, TfR1, FPN, FTH and FTL in liver tissues (n = 4–6). (D) The protein expression of FTH, FTL and TfR1 in Hep-G2 cells. (E) The quantification of protein expression (n = 3–4). (F) The mRNA levels of DMT1, TfR1, FPN, FTH and FTL in Hep-G2 cells (n = 4–6). Data were presented by the mean ± SEM. *P<0.05; **P<0.01; ***P<0.001; NS refers to non-significant.

pivotal upstream regulator of Nrf2 nuclear export [35]. Activated GSK3β promotes the degradation and nuclear export of Nrf2, consequently reducing the protein abundance of Nrf2 within the nucleus [35,36]. We measured the phosphorylation level of GSK3β at the Ser-9 site, an inhibitory site for the activation of GSK3β. Interestingly, we found that Lira and GLP-1(9–37) treatments significantly increased the phosphorylation level at the Ser-9 site compared to the Control and H/R groups (Fig. 7L). To investigate whether the inhibitory effect of Lira and GLP-1 (9–37) on Nrf2 nuclear export is related to the phosphorylation of GSK3β, we utilized DIF-3 to inhibit the phosphorylation level of GSK3β at the Ser-9 site and the results showed that the effect of Lira and GLP-1 (9–37) on increasing Nrf2 nuclear abundance was reversed by the inhibition of GSK3β phosphorylation (Fig. 7M). Besides, we employed Molecular docking to predict the binding affinity between GLP-1R and GSK3β, as well as between GLP-1(9–37) and GSK3β. The confidence score and binding energy indicated that both GLP-1R and GLP-1(9–37) might have a good binding affinity to GSK3β (Fig. 7N). The potential binding sites were shown in Fig. S7 (Figs. S7A and C). The result of IP also indicated the interaction between GLP-1R and GSK3β (Fig. 7O). These findings suggested that the promoted nuclear translocation of Nrf2 induced by Lira and GLP-1(9–37) might be mediated through the modulation of GSK3β activity.

3.8. Lira and GLP-1(9–37) increased the expression of FTH and FTL in HIRI and H/R models

Iron plays a pivotal role in the initiation of ferroptosis. Thus, besides enhancing antioxidant capacity, reducing intracellular free iron levels can also effectively hinder the progression of ferroptosis [37]. Intracellular iron levels are regulated by the proteins associated with iron metabolism, such as iron transporters (TfR1, DMT1, FPN) and iron storage proteins (FTH, FTL) [38]. In this study, our results have indicated that Lira and GLP-1(9–37) could significantly decrease the levels of Fe^{2+} in both the HIRI model and the H/R model, and the GO analysis of both groups enriched the iron ion binding function. To explore the underlying mechanism of the decreased Fe^{2+} levels, we further conducted a analysis of the proteins linked to iron metabolism. In mouse liver tissues, Lira and GLP-1(9–37) preconditioning significantly enhanced the expression of FTH and FTL at both protein and mRNA levels in comparison to the I/R group; however, there was no alteration in the levels of TfR1, FPN and DMT1 (Fig. 8A, B, C). Similarly, in the H/R model, the expression trends were consistent with those observed in the HIRI model, except for an observed increase in both the protein and mRNA levels of TfR1 induced by GLP-1(9–37) treatment (Fig. 8D, E, F). These results suggested that Lira and GLP-1(9–37) might reduce the intracellular Fe^{2+} levels by increasing the FTH and FTL expression.

3.9. Lira and GLP-1(9–37) increased the expression of FTH and FTL via the SMAD159/Hepcidin pathway

The levels of FTH and FTL can be regulated by many factors, such as ferritinophagy, iron-regulatory proteins (IRPs) and hepcidin, etc [39–41]. Ferritinophagy can lead to the degradation of FTH, resulting in an increase in Fe^{2+} levels [39]. IRPs can bind to the 5' UTR of FTH and FTL mRNAs and prevent their translation [40]. Hepcidin, primarily secreted by the liver, is an iron regulatory hormone that regulates both systemic and intracellular iron metabolism [42]. Recent studies have demonstrated that Hepcidin can enhance the expression of FTH, thereby inhibiting ferroptosis [41]. To explore the mechanisms by which Lira and GLP-1(9–37) increase the expression of FTH and FTL, we examined these three aspects respectively.

Initially, we detected the expression of NCOA4, LC3 and P62 in liver tissues and Hep-G2 cells. Our findings suggested that the administration of Lira and GLP-1(9–37) seemed not to result in a significant change in ferritinophagy levels compared to the I/R or H/R groups (Figs. S5A and S5B). A similar result was observed after inhibiting lysosomal activity by bafilomycin A1 (Fig. S5E). Subsequent examination of IRP1 and IRP2 expression indicated that Lira and GLP-1(9–37) had no effect on IRP1 and IRP2 levels in liver tissues compared to the I/R group, while in Hep-G2 cells, they increased IRP1 expression but did not affect IRP2 expression compared to the H/R group (Figs. S5C and S5D). Furthermore, We evaluated the binding activity of IRP1 to FTH and FTL mRNA in the Hep-G2 cells treated with Lira and GLP-1(9–37). The results showed that treatment with Lira and GLP-1(9–37) seemed to inhibit the binding of IRP1 to FTH and FTL mRNA compared to the Control group, but it was not statistically significant (Fig. S5F). Finally, we conducted an analysis of Hepcidin (encoded by HAMP) at both the protein and mRNA levels in liver tissues. The results demonstrated a reduction in Hepcidin levels following I/R, while preconditioning with Lira and GLP-1(9–37) significantly increased hepcidin expression (Fig. 8A, B, 9A). This trend was consistent with that of FTH and FTL, so we speculated that Lira and GLP-1(9–37) might promote the expression of FTH and FTL by increasing Hepcidin expression.

To investigate whether the increased expression of FTH and FTL induced by Lira and GLP-1(9–37) is related to the increased Hepcidin, we utilized Hepcidin antagonist-1 to block the function of Hepcidin. The results showed that the increases in FTH and FTL induced by Lira and GLP-1(9–37) were significantly reversed after using Hepcidin antagonist-1 (Fig. 9B). Meanwhile, the protective effects of Lira and GLP-1(9–37), as well as their effects on intracellular ROS, oxidized lipids, Fe^{2+} and GPX4 expression were significantly countered (Fig. 9C, D, E, F, G). These findings suggested that Lira and GLP-1(9–37) might increase FTH and FTL expression by the increased hepcidin, thereby improving iron metabolism and inhibiting ferroptosis.

It has been established that the activation of the STAT3 pathway and SMAD159 (also known as SMAD158) pathway is correlated with the increased Hepcidin expression [43]. First, we examined the activation of the STAT3 pathway. The results revealed a significant increase in phosphorylated STAT3 (p-STAT3) following I/R; however, there was no statistically significant difference in p-STAT3 expression following the preconditioning with Lira and GLP-1(9–37) compared to the I/R group (Fig. 9H). Subsequently, we examined the activation of the SMAD159 pathway and observed a notable reduction in SMAD159 expression in mouse liver tissues post-I/R, which was reversed by the Lira and GLP-1 (9–37) preconditioning (Fig. 9I). Next, we further examined the downstream changes of this pathway. Following I/R, both nuclear and cytoplasmic SMAD4 protein levels were decreased, while the preconditioning with Lira and GLP-1(9–37) resulted in a notable increase in the nuclear SMAD4 protein levels, without affecting the cytoplasmic SMAD4 protein levels (Fig. 9J). This result indicated that Lira and GLP-1(9–37) promoted the nuclear translocation of SMAD4, which was consistent with the changes observed in the activation of the SMAD159 pathway. Finally, we examined the expression of the downstream genes in this pathway. In addition to HAMP, the mRNA levels of SMAD7 and Id1 were also increased (Fig. 9K), which suggested the activation of the SMAD159 pathway [44]. These results suggested that the SMAD159 pathway was activated by Lira and GLP-1(9–37) treatments. To investigate whether the increased hepcidin induced by Lira and GLP-1(9–37) is related to the activated SMAD159 pathway, we then utilized LDN193189 to inhibit the SMAD159 pathway. The specific dosing regimen was shown in Fig. 9L (Fig. 9L). The results revealed a marked decrease in hepcidin expression with LDN193189 treatment; meanwhile, the increased expression of FTH and FTL induced by Lira and GLP-1(9–37) was significantly reversed (Fig. 9M). Additionally, we also employed Molecular docking to predict the binding affinity between GLP-1R and SMAD159, as well as between GLP-1(9–37) and SMAD159, and the confidence score and binding energy indicated that both GLP-1R and GLP-1(9–37) might have a good binding affinity to SMAD159 (Fig. 9N). The potential binding sites were shown in Fig. S7 (Figs. S7B and D). The result of IP also indicated the interaction between GLP-1R and SMAD159 (Fig. 9O). These findings indicated that Lira and GLP-1(9–37) could increase the expression of FTH and FTL through the

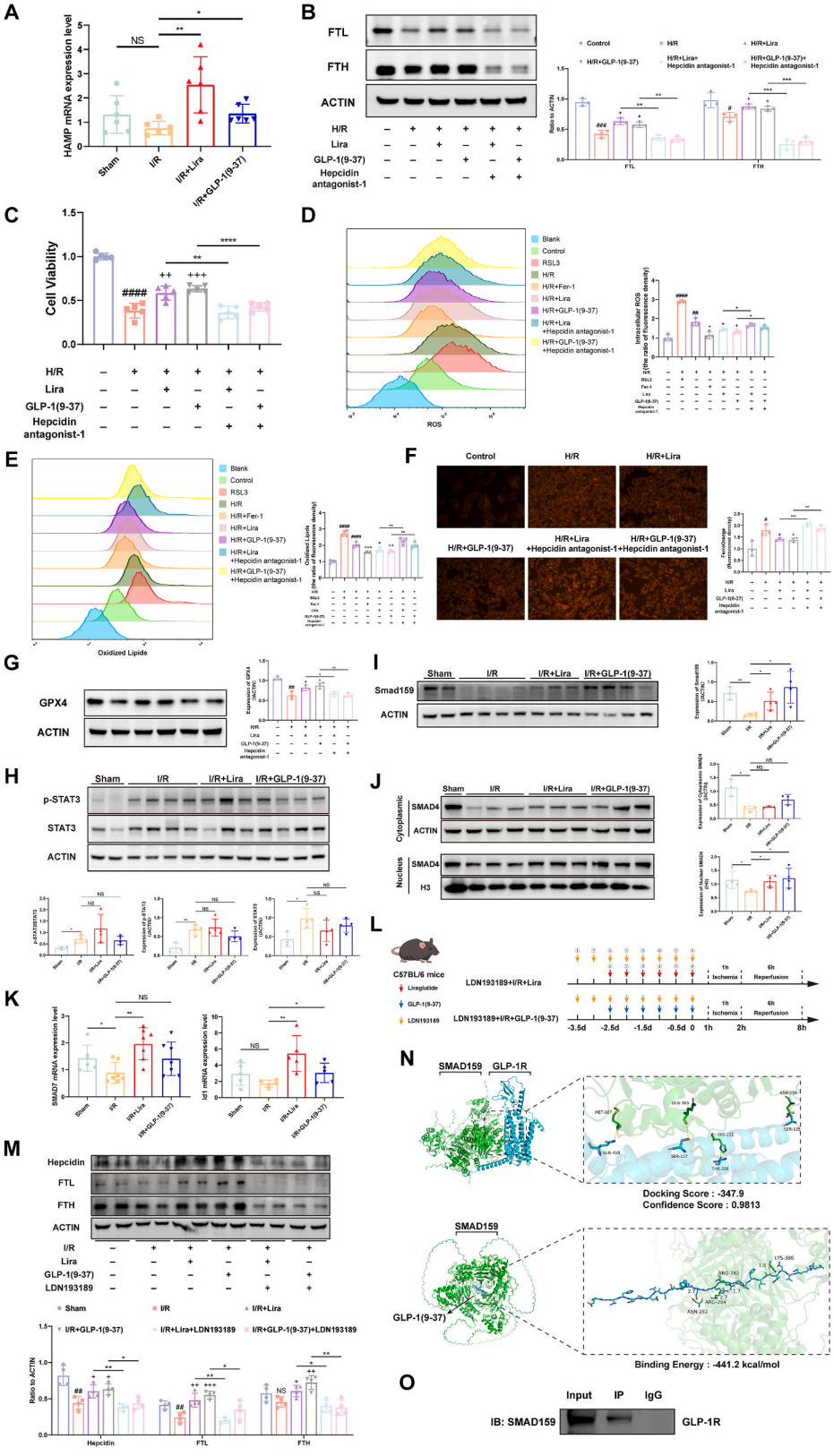

(caption on next page)

Fig. 9. Liraglutide and GLP-1(9–37) increased the expression of FTH and FTL by activating the SMAD159/Hepcidin pathway.
(A) The mRNA level of HAMP in liver tissues (n = 6). (B) The protein expression of FTH and FTL in Hep-G2 cells following hepcidin inhibition by hepcidin antagonist-1 (3 μM) was measured by WB, and the quantitative result was performed (n = 3). (C) The cell viability was measured by CCK-8 kit (n = 5). (D) Intracellular ROS of each group was measured by flow cytometry and the quantification of ROS level was shown (n = 3). (E) The oxidized lipids in cells of each group were detected by flow cytometry using C11-BODIPY probe and the ratio of fluorescence density was shown (n = 4). (F) The Fe^{2+} in cells was observed by FerroOrange probe and the fluorescence density was performed (n = 3). (G) The protein level of GPX4 in cells of each group was detected and the quantification was performed (n = 3). (H) The protein expression of STAT3 and p-STAT3 in liver tissues was measured by Western blot and the quantification was performed (n = 3–4). (I) The protein expression of SMAD159 in liver tissues was measured and the quantification was performed (n = 3–4). (J) The protein expression of SMAD4 in cytoplasm and nucleus in liver tissues was measured by Western blot and the quantification was performed (n = 3–4). (K) The mRNA levels of SMAD7 and Id1 in liver tissues (n = 5–6). (L) Detailed treatment in vivo. Red arrows refer to liraglutide (200 μg/kg), blue arrows refer to GLP-1(9–37) (200 μg/kg) and yellow arrows refer to LDN193189 (3 mg/kg). (M) The protein expression of Hepcidin, FTH and FTL in liver tissues was observed by Western blot and the quantification was performed (n = 4). (N) Molecular docking proposed the interaction mode of GLP-1R and SMAD159 (Docking Score: −347.9; Confidence Score: 0.9813) and the interaction mode of GLP-1(9–37) and SMAD159 (Binding Energy: −441.2 kcal/mol). (O) The interaction between GLP-1R and SMAD159 was detected by immunoprecipitation. Data were presented by the mean ± SEM. $^{\#\#}P<0.01$ versus the Sham group; $^{+}P<0.05$, $^{++}P<0.01$, $^{+++}P<0.001$ versus the I/R group; $^{*}P<0.05$; $^{**}P<0.01$; NS refers to non-significant.

SMAD159/Hepcidin pathway.

4. Discussion

Ferroptosis, recognized as an emerging form of cellular demise, has been implicated in a multitude of diseases. Studies have extensively documented that a substantial accumulation of iron and lipid peroxides appear in liver tissues following I/R, and that ferroptosis inhibitors can effectively alleviate HIRI, indicating ferroptosis as a promising therapeutic target for HIRI [11–13]. In this study, we identified that both Liraglutide and its metabolite GLP-1(9–37) alleviated the liver injury induced by I/R in mice and improved the impaired viability of Hep-G2 cells induced by H/R through the inhibition of ferroptosis.

The excessive presence of iron and the accumulation of lipid peroxides are the two primary factors precipitating the occurrence of ferroptosis. Within these two factors, the accumulation of lipid peroxides on the plasma membrane serves as the immediate trigger for the execution of ferroptosis, while the excessive iron catalyzes and accelerates this process, heightening the cell's susceptibility to ferroptosis [7,45]. It follows that the scavenging of accumulated lipid peroxides by enhancing antioxidant capacity and the reduction of excessive free iron within cells can both exert an inhibitory impact on ferroptosis. In this investigation, we explored the mechanism by which Liraglutide and GLP-1(9–37) inhibited ferroptosis during hepatic ischemia-reperfusion. On one hand, they enhanced the cellular antioxidant capacity via the GSK3β/Nrf2 pathway, leading to a decrease in lipid peroxide accumulation. On the other hand, they reduced the levels of free iron through the SMAD159/Hepcidin/FTH pathway. These two effects may elucidate the inhibitory effect of Liraglutide and GLP-1(9–37) on ferroptosis. However, whether these two mechanisms act independently or interact with each other remains to be investigated.

Nrf2 plays a crucial role in regulating intracellular antioxidant capacity. As a transcription factor, Nrf2 can translocate from the cytoplasm to the nucleus and then interact with the antioxidant response elements to enhance the expression of antioxidant enzymes including HO-1, NQO1 and so on, thereby inhibiting the occurrence of lipid peroxidation [46]. Studies have shown that decreasing Nrf2 levels can heighten the sensitivity of cancer cells to ferroptosis inducers [47], while activating the Nrf2 pathway can prevent the occurrence of ferroptosis [46,48]. Previous research has demonstrated that Liraglutide can activate the Nrf2 pathway to exert antioxidant effects [49]. However, there is also a report suggesting that it can reduce the aggregation of Nrf2 in the nucleus induced by endoplasmic reticulum (ER) stress and autophagy impairments [50]. In our study, we observed that Liraglutide enhanced the nuclear translocation of Nrf2 and increased the expression of downstream antioxidant enzymes in mouse livers and Hep-G2 cells, which was consistent with the majority of previous studies. Additionally, we also found that its metabolite GLP-1(9–37) exhibited a similar effect. Meanwhile, the effects of Liraglutide and GLP-1(9–37) on HIRI and on the reduction of lipid peroxides were weakened when ML385, an inhibitor of the Nrf2 pathway, was utilized. Therefore, we believed that the effects of Liraglutide and GLP-1(9–37) on reducing lipid peroxides were associated with the activation of the Nrf2 pathway. The decrease in nuclear Nrf2 levels observed in the previous study may be a consequence of improved ER stress and autophagy, rather than a direct effect of Liraglutide. GSK3β is an important molecule that regulates the nuclear export of Nrf2. Its active form (low phosphorylation at the Ser-9 site) can promote the translocation of Nrf2 from the nucleus to the cytoplasm [51]. Our results indicated that the increased Nrf2 abundance in the nucleus induced by Liraglutide and GLP-1(9–37) might be associated with the inhibition of GSK3β activity. Liraglutide, as a GLP-1R agonist, might be able to influence the phosphorylation of GSK3β by activating GLP-1R, while GLP-1(9–37), as a metabolite with low affinity for GLP-1R, might exert its effects by directly acting on GSK3β.

The homeostasis of intracellular iron is orchestrated by iron transporters (TfR1, DMT1, FPN, etc.) and iron storage proteins (FTH, FTL, etc.). TfR1 and DMT1 can convert the Fe^{3+} bound with transferrin into Fe^{2+} and transport it into the cytoplasm to form the labile iron pool (LIP), while FPN can transport the excessive intracellular iron into the extracellular milieu; FTH and FTL, as iron storage proteins, can bind to the Fe^{2+} within the LIP and store it in the form of Fe^{3+}, thereby reducing the abundance of free iron within the cell [38]. Previous studies have demonstrated that increasing FTH and FTL expression can enhance the cellular resistance against ferroptosis [52,53]. A previous study showed that administration of Liraglutide led to an elevation in FTH and FPN expression and a decline in TfR1 expression, but no significant change in FTL [54]. In the present study, we also evaluated the expression of these proteins and observed that both Liraglutide and GLP-1(9–37) elevated the levels of FTH in mouse liver tissues and Hep-G2 cells, aligning with the findings from prior research. However, the level of FTL was also increased and the level of TfR1 remained unchanged in our investigation. This inconsistency in results may be ascribed to variations in disease models and dosage regimens employed across the distinct studies. The intricate regulation of FTH and FTL expression involves diverse mechanisms, such as ferritinophagy, IRPs and hepcidin [39–41]. However, to our knowledge, the mechanism by which Liraglutide and GLP-1 (9–37) regulate the expression of FTH and FTL has not been reported. In our study, we found that Liraglutide and GLP-1(9–37) seemed to have no significant effect on ferritinophagy and IRPs, but they increased the expression of hepcidin. It has been found in a study that hepcidin could lead to an increase in FTH expression, thereby inhibiting the occurrence of ferroptosis [41]. Thus, we speculated that hepcidin might be a reason for the increased expression of FTH and FTL induced by Liraglutide and GLP-1(9–37). Further, we examined the activation of the STAT3 pathway and the SMAD159 pathway, the two major pathways regulating the expression of hepcidin [43]. We found that both Liraglutide and GLP-1(9–37) activated the SMAD159 pathway, while they did not exhibit a significant impact on the STAT3 pathway. Additionally, LDN193189, an inhibitor of the SMAD159/Hepcidin pathway, effectively counteracted the heightened expression of FTH and FTL induced by Liraglutide and GLP-1(9–37). Hence, we believed that Liraglutide and GLP-1(9–37) increased the expression of FTH and FTL via the

SMAD159/Hepcidin pathway, thereby regulating intracellular free iron levels. Additionally, the present study also indicated that Liraglutide, as a GLP-1R agonist, might be able to influence the protein level of SMAD159 by activating GLP-1R, while GLP-1(9–37), as a metabolite with low affinity for GLP-1R, might exert its effects by directly acting on SMAD159.

However, the detailed mechanisms by which liraglutide and GLP-1 (9–37) affect the activities of GSK3β and SMAD159 require further investigation. Previous studies have found that the phosphorylation of GSK3β at the Ser-9 site could be regulated by the actions of other sites, such as Arg-4 and Arg-141 [55,56]. Thus, based on our molecular docking data, we speculate that activated GLP-1R and GLP-1(9–37) may influence the phosphorylation of GSK3β by acting on the Arg4 and Arg141 sites, respectively, thereby affecting its activity. In the present study, we observed that Liraglutide and GLP-1(9–37) significantly reversed the decrease in SMAD159 caused by I/R. Given that the proteasomal degradation system is enhanced during I/R and that activated GLP-1R can inhibit protein ubiquitination [57,58], we speculate that Liraglutide may activate the SMAD159 pathway by reducing the ubiquitin-mediated degradation of SMAD159.

Liraglutide, which shares a 97 % sequence similarity to the native GLP-1, is supposed to exert its effects by activating the GLP-1R. However, our previous studies have revealed that Liraglutide still retains a partially protective effect against disease in GLP-1R$^{-/-}$ mice [24,59]. This phenomenon suggests that a portion of the effect of Liraglutide may occur independently of GLP-1R. GLP-1(9–37), as a metabolite of GLP-1, exhibits a very low affinity for GLP-1R, but still has some biological effects. Thus, this metabolite is thought to be one of the reasons why Liraglutide is able to function independently of GLP-1R [60,61]. In this study, we discovered that besides Liraglutide, GLP-1(9–37) also exhibited an inhibitory effect on ferroptosis in HIRI. This discovery prompted us to speculate that the effect of Liraglutide on ferroptosis could also be mediated by a GLP-1R-independent pathway. To verify this hypothesis, we employed GLP-1R$^{-/-}$ mice and discovered that both Liraglutide and GLP-1(9–37) still mitigated the ferroptosis in HIRI in the absence of the GLP-1R, although the effect was attenuated. Consequently, we believed that Liraglutide could inhibit the ferroptosis in HIRI through both GLP-1R-dependent and GLP-1R-independent pathways. Nevertheless, the specific mechanism underlying the GLP-1R-independent pathway remains to be investigated.

In summary, as depicted in Fig. 10, the research revealed that Liraglutide and its metabolite GLP-1(9–37) inhibited the ferroptosis in HIRI through the GSK3β/Nrf2 pathway and the SMAD159/Hepcidin/FTH pathway, and the effect of Liraglutide was mediated by both GLP-1R-dependent and GLP-1R-independent pathways. Although the relationship between Liraglutide and ferroptosis has been explored in a few recent literatures, the specific mechanism by which Liraglutide affects the iron metabolism has not been explained [23,54,62]. This study explored the mechanism behind the reduction of Fe^{2+} levels by Liraglutide and GLP-1(9–37), proposing that the enhanced expression of FTH and FTL induced by the activation of the SMAD159/Hepcidin pathway was one of the contributing factors.

However, this study does have some limitations. Firstly, in addition to hepatocytes, the liver contains various other cell types, such as

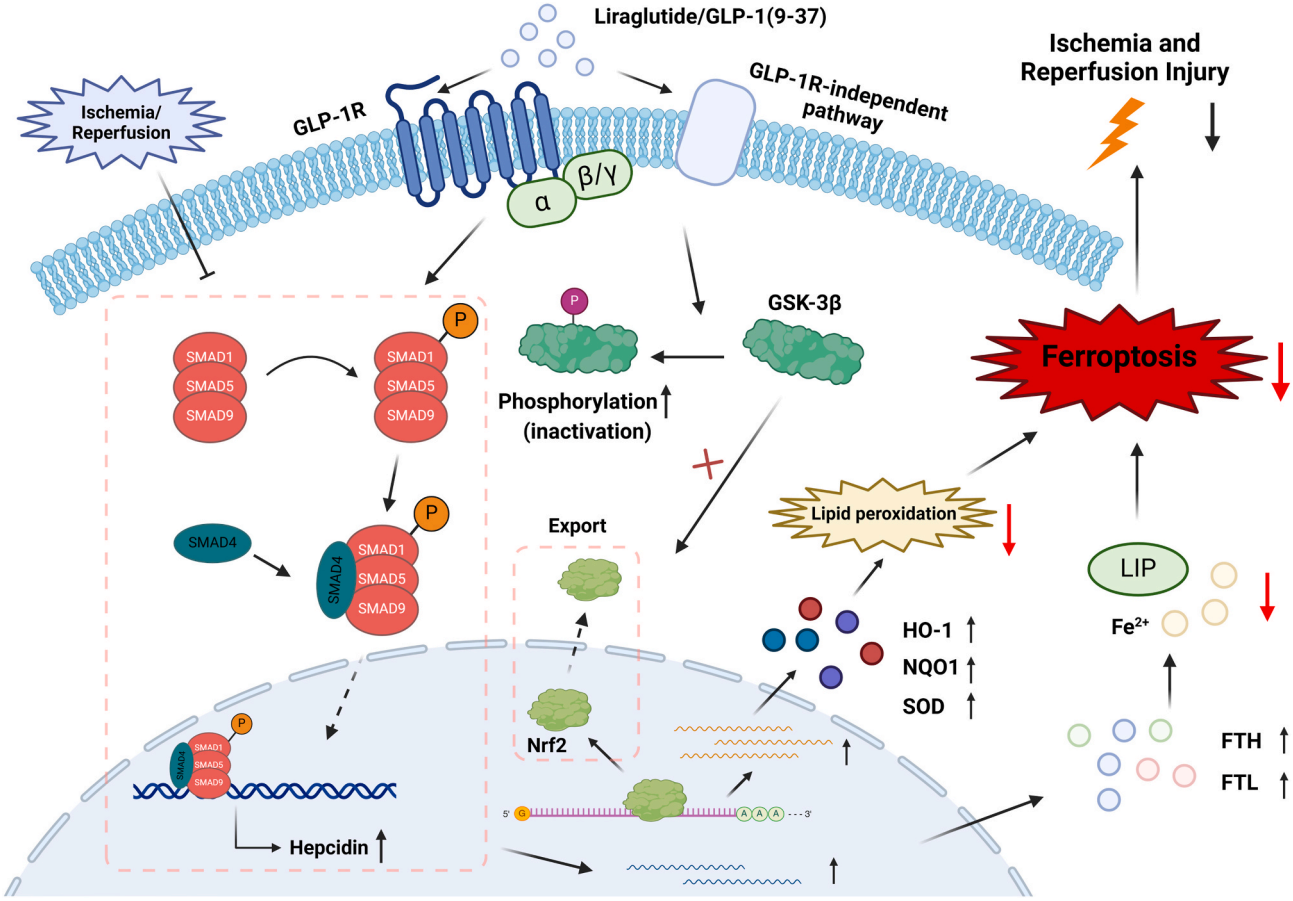

Fig. 10. The summary of the mechanisms by which Lira and GLP-1(9–37) attenuate the ferroptosis in HIRI.
On one hand, Lira and GLP-1(9–37) inhibit the activity of GSK3β by promoting its phosphorylation, which leads to the inhibition of Nrf2 export and its retention in the nucleus; the increased Nrf2 in the nucleus leads to an increase of antioxidant enzymes and therefore alleviates the lipid peroxidation in HIRI. On the other hand, they activate the SMAD159/Hepcidin pathway, resulting in an increase of hepcidin; the increased hepcidin promotes the expression of FTH and FTL, which leads to a decrease of Fe^{2+} in HIRI. Through these two effects, Lira and GLP-1(9–37) attenuate the ferroptosis, thereby improving HIRI. This figure was created with BioRender.

hepatic stellate cells and kupffer cells. However, the assessment of the ferroptosis-related indicators from these cells was not conducted in this study. Secondly, the specific mechanism underlying the GLP-1R-independent effect of Liraglutide was not further explored. Thirdly, a detailed comparison of the *anti*-ferroptosis effects between Liraglutide and GLP-1(9–37) requires further study. Finally, the more detailed mechanisms through which Liraglutide and GLP-1(9–37) influence the activation of GSK3β and the protein level of SMAD159 remain unclear and require further investigation.

This study determined the effects of Liraglutide and GLP-1(9–37) on iron metabolism, which provided a new sight into their biological effects. We believed that as a drug widely used in clinical practice, Liraglutide is expected to be further applied in treating liver diseases associated with iron metabolism disorders. Additionally, GLP-1(9–37), as a metabolite of Liraglutide, also has significant potential for clinical transformation.

CRediT authorship contribution statement

Chenqi Lu: Writing – original draft, Visualization, Validation, Methodology, Investigation, Formal analysis, Data curation, Conceptualization. **Cong Xu:** Writing – original draft, Visualization, Validation, Formal analysis, Data curation. **Shanglin Li:** Visualization, Validation, Data curation. **Haiqiang Ni:** Writing – review & editing, Supervision, Resources, Project administration, Methodology, Investigation, Funding acquisition, Conceptualization. **Jun Yang:** Writing – review & editing, Supervision, Software, Resources, Project administration, Methodology, Investigation, Funding acquisition, Conceptualization.

Funding

This study was funded by the National Natural Science Foundation of China (81873624).

Declaration of competing interest

The authors declare that they have no known competing financial interests or personal relationships that could have appeared to influence the work reported in this paper.

Acknowledgements

We sincerely acknowledge Xiaofan Hu, Yang Qiu, Rui Cao, Yanan Xie for their support in various aspects of this study.

Appendix A. Supplementary data

Supplementary data to this article can be found online at https://doi.org/10.1016/j.redox.2024.103468.

Data availability

Data will be made available on request.

References

[1] G.J. Nieuwenhuijs-Moeke, S.E. Pischke, S.P. Berger, et al., Ischemia and reperfusion injury in kidney transplantation: relevant mechanisms in injury and repair, J. Clin. Med. 9 (1) (2020).
[2] R.E.D.P. Del, D. Amgalan, A. Linkermann, et al., Fundamental mechanisms of regulated cell death and implications for heart disease, Physiol. Rev. 99 (4) (2019) 1765–1817.
[3] Y. Pan, X. Wang, X. Liu, et al., Targeting ferroptosis as a promising therapeutic strategy for ischemia-reperfusion injury, Antioxidants 11 (11) (2022).
[4] E.B. Thorgersen, A. Barratt-Due, H. Haugaa, et al., The role of complement in liver injury, regeneration, and transplantation, Hepatology 70 (2) (2019) 725–736.
[5] B. Mao, W. Yuan, F. Wu, et al., Autophagy in hepatic ischemia-reperfusion injury, Cell Death Dis. 9 (1) (2023) 115.
[6] S.J. Dixon, K.M. Lemberg, M.R. Lamprecht, et al., Ferroptosis: an iron-dependent form of nonapoptotic cell death, Cell 149 (5) (2012) 1060–1072.
[7] J. Li, F. Cao, H.L. Yin, et al., Ferroptosis: past, present and future, Cell Death Dis. 11 (2) (2020) 88.
[8] X. Jiang, B.R. Stockwell, M. Conrad, Ferroptosis: mechanisms, biology and role in disease, Nat. Rev. Mol. Cell Biol. 22 (4) (2021) 266–282.
[9] D. Tang, X. Chen, R. Kang, et al., Ferroptosis: molecular mechanisms and health implications, Cell Res. 31 (2) (2021) 107–125.
[10] M. Liu, X.Y. Kong, Y. Yao, et al., The critical role and molecular mechanisms of ferroptosis in antioxidant systems: a narrative review, Ann. Transl. Med. 10 (6) (2022) 368.
[11] N. Yamada, T. Karasawa, T. Wakiya, et al., Iron overload as a risk factor for hepatic ischemia-reperfusion injury in liver transplantation: potential role of ferroptosis, Am. J. Transplant. 20 (6) (2020) 1606–1618.
[12] L. Luo, G. Mo, D. Huang, Ferroptosis in hepatic ischemia-reperfusion injury: regulatory mechanisms and new methods for therapy (Review), Mol. Med. Rep. 23 (3) (2021).
[13] J. Junzhe, L. Meng, H. Weifan, et al., Potential effects of different cell death inhibitors in protecting against ischemia-reperfusion injury in steatotic liver, Int. Immunopharm. 128 (2024) 111545.
[14] L.B. Knudsen, J. Lau, The discovery and development of liraglutide and semaglutide, Front. Endocrinol. 10 (2019) 155.
[15] L.V. Jacobsen, A. Flint, A.K. Olsen, et al., Liraglutide in type 2 diabetes mellitus: clinical pharmacokinetics and pharmacodynamics, Clin. Pharmacokinet. 55 (6) (2016) 657–672.
[16] X. Zhao, M. Wang, Z. Wen, et al., GLP-1 receptor agonists: beyond their pancreatic effects, Front. Endocrinol. 12 (2021) 721135.
[17] M.A. Nauck, J.J. Meier, M.A. Cavender, et al., Cardiovascular actions and clinical outcomes with glucagon-like peptide-1 receptor agonists and dipeptidyl peptidase-4 inhibitors, Circulation 136 (9) (2017) 849–870.
[18] E.V. Greco, G. Russo, A. Giandalia, et al., GLP-1 receptor agonists and kidney protection, Medicina (Kaunas) 55 (6) (2019).
[19] A. Mantovani, G. Petracca, G. Beatrice, et al., Glucagon-like peptide-1 receptor agonists for treatment of nonalcoholic fatty liver disease and nonalcoholic steatohepatitis: an updated meta-analysis of randomized controlled trials, Metabolites 11 (2) (2021).
[20] Z. Zou, Z. Wang, Liraglutide attenuates intestinal ischemia/reperfusion injury via NF-κB and PI3K/Akt pathways in mice, Life Sci. 309 (2022) 121045.
[21] S. Song, R. Guo, A. Mehmood, et al., Liraglutide attenuate central nervous inflammation and demyelination through AMPK and pyroptosis-related NLRP3 pathway, CNS Neurosci. Ther. 28 (3) (2022) 422–434.
[22] X. Han, C. Ding, G. Zhang, et al., Liraglutide ameliorates obesity-related nonalcoholic fatty liver disease by regulating Sestrin2-mediated Nrf2/HO-1 pathway, Biochem. Biophys. Res. Commun. 525 (4) (2020) 895–901.
[23] J.X. Song, J.R. An, Q. Chen, et al., Liraglutide attenuates hepatic iron levels and ferroptosis in db/db mice, Bioengineered 13 (4) (2022) 8334–8348.
[24] C. Xu, C. Lu, Z. Wang, et al., Liraglutide abrogates nephrotoxic effects of chemotherapies, Pharmacol. Res. 189 (2023) 106680.
[25] J.R. Ussher, L.L. Baggio, J.E. Campbell, et al., Inactivation of the cardiomyocyte glucagon-like peptide-1 receptor (GLP-1R) unmasks cardiomyocyte-independent GLP-1R-mediated cardioprotection, Mol. Metabol. 3 (5) (2014) 507–517.
[26] K. Ban, M.H. Noyan-Ashraf, J. Hoefer, et al., Cardioprotective and vasodilatory actions of glucagon-like peptide 1 receptor are mediated through both glucagon-like peptide 1 receptor-dependent and -independent pathways, Circulation 117 (18) (2008) 2340–2350.
[27] G. Cantini, E. Mannucci, M. Luconi, Perspectives in GLP-1 research: new targets, new receptors, Trends Endocrinol. Metabol. 27 (6) (2016) 427–438.
[28] R. Sharma, T.S. Mcdonald, H. Eng, et al., In vitro metabolism of the glucagon-like peptide-1 (GLP-1)-derived metabolites GLP-1(9-36)amide and GLP-1(28-36)amide in mouse and human hepatocytes, Drug Metab. Dispos. 41 (12) (2013) 2148–2157.
[29] V. Guglielmi, P. Sbraccia, GLP-1 receptor independent pathways: emerging beneficial effects of GLP-1 breakdown products, Eat. Weight Disord. 22 (2) (2017) 231–240.
[30] Z. Zou, R. Shang, L. Zhou, et al., The novel MyD88 inhibitor TJ-m2010-5 protects against hepatic ischemia-reperfusion injury by suppressing pyroptosis in mice, Transplantation 107 (2) (2023) 392–404.
[31] S. Suzuki, L.H. Toledo-Pereyra, F.J. Rodriguez, et al., Neutrophil infiltration as an important factor in liver ischemia and reperfusion injury. Modulating effects of FK506 and cyclosporine, Transplantation 55 (6) (1993) 1265–1272.
[32] A. Cameron-Vendrig, A. Reheman, M.A. Siraj, et al., Glucagon-like peptide 1 receptor activation attenuates platelet aggregation and thrombosis, Diabetes 65 (6) (2016) 1714–1723.
[33] S. Sajadimajd, M. Khazaei, Oxidative stress and cancer: the role of Nrf2, Curr. Cancer Drug Targets 18 (6) (2018) 538–557.
[34] B.C. Kuang, Z.H. Wang, S.H. Hou, et al., Methyl eugenol protects the kidney from oxidative damage in mice by blocking the Nrf2 nuclear export signal through activation of the AMPK/GSK3β axis, Acta Pharmacol. Sin. 44 (2) (2023) 367–380.
[35] F. Farhat, S. Nofal, E.M. Raafat, et al., Akt/GSK3β/Nrf2/HO-1 pathway activation by flurbiprofen protects the hippocampal neurons in a rat model of glutamate excitotoxicity, Neuropharmacology 196 (2021) 108654.
[36] S. Liao, J. Wu, R. Liu, et al., A novel compound DBZ ameliorates neuroinflammation in LPS-stimulated microglia and ischemic stroke rats: role of Akt(Ser473)/GSK3β(Ser9)-mediated Nrf2 activation, Redox Biol. 36 (2020) 101644.

[37] L. Rochette, G. Dogon, E. Rigal, et al., Lipid peroxidation and iron metabolism: two corner stones in the homeostasis control of ferroptosis, Int. J. Mol. Sci. 24 (1) (2022).
[38] G. Gao, J. Li, Y. Zhang, et al., Cellular iron metabolism and regulation, Adv. Exp. Med. Biol. 1173 (2019) 21–32.
[39] W. Hou, Y. Xie, X. Song, et al., Autophagy promotes ferroptosis by degradation of ferritin, Autophagy 12 (8) (2016) 1425–1428.
[40] N. Sukhbaatar, T. Weichhart, Iron regulation: macrophages in control, Pharmaceuticals 11 (4) (2018).
[41] Y. Jiao, C. Yong, R. Zhang, et al., Hepcidin alleviates LPS-induced ARDS by regulating the ferritin-mediated suppression of ferroptosis, Shock 57 (6) (2022) 274–281.
[42] E. Nemeth, T. Ganz, Hepcidin and iron in health and disease, Annu. Rev. Med. 74 (2023) 261–277.
[43] A.S. Vogt, T. Arsiwala, M. Mohsen, et al., On iron metabolism and its regulation, Int. J. Mol. Sci. 22 (9) (2021).
[44] L. Kautz, D. Meynard, A. Monnier, et al., Iron regulates phosphorylation of Smad1/5/8 and gene expression of Bmp6, Smad7, Id1, and Atoh8 in the mouse liver, Blood 112 (4) (2008) 1503–1509.
[45] S.J. Dixon, J.A. Olzmann, The cell biology of ferroptosis, Nat. Rev. Mol. Cell Biol. 25 (6) (2024) 424–442.
[46] M. Dodson, R. Castro-Portuguez, D.D. Zhang, NRF2 plays a critical role in mitigating lipid peroxidation and ferroptosis, Redox Biol. 23 (2019) 101107.
[47] Z. Fan, A.K. Wirth, D. Chen, et al., Nrf2-Keap1 pathway promotes cell proliferation and diminishes ferroptosis, Oncogenesis 6 (8) (2017) e371.
[48] Y. Baba, J.K. Higa, B.K. Shimada, et al., Protective effects of the mechanistic target of rapamycin against excess iron and ferroptosis in cardiomyocytes, Am. J. Physiol. Heart Circ. Physiol. 314 (3) (2018) H659–h68.
[49] C.G. Zhu, Y. Luo, H. Wang, et al., Liraglutide ameliorates lipotoxicity-induced oxidative stress by activating the NRF2 pathway in HepG2 cells, Horm. Metab. Res. 52 (7) (2020) 532–539.
[50] T. Panagaki, M. Michael, C. HöLSCHER, Liraglutide restores chronic ER stress, autophagy impairments and apoptotic signalling in SH-SY5Y cells, Sci. Rep. 7 (1) (2017) 16158.
[51] A.K. Jain, A.K. Jaiswal, GSK-3beta acts upstream of Fyn kinase in regulation of nuclear export and degradation of NF-E2 related factor 2, J. Biol. Chem. 282 (22) (2007) 16502–16510.
[52] W. Hu, C. Zhou, Q. Jing, et al., FTH promotes the proliferation and renders the HCC cells specifically resist to ferroptosis by maintaining iron homeostasis, Cancer Cell Int. 21 (1) (2021) 709.
[53] X. Yang, Y. Ding, L. Sun, et al., Ferritin light chain deficiency-induced ferroptosis is involved in preeclampsia pathophysiology by disturbing uterine spiral artery remodelling, Redox Biol. 58 (2022) 102555.
[54] J.R. An, J.N. Su, G.Y. Sun, et al., Liraglutide alleviates cognitive deficit in db/db mice: involvement in oxidative stress, iron overload, and ferroptosis, Neurochem. Res. 47 (2) (2022) 279–294.
[55] R. Ilouz, S. Pietrokovski, M. Eisenstein, et al., New insights into the autoinhibition mechanism of glycogen synthase kinase-3beta, J. Mol. Biol. 383 (5) (2008) 999–1007.
[56] N. Yan, F. Xie, L.Q. Tang, et al., Synthesis and biological evaluation of thieno[3,2-c]pyrazol-3-amine derivatives as potent glycogen synthase kinase 3β inhibitors for Alzheimer's disease, Bioorg. Chem. 138 (2023) 106663.
[57] Q. Xia, G. Zhan, M. Mao, et al., TRIM45 causes neuronal damage by aggravating microglia-mediated neuroinflammation upon cerebral ischemia and reperfusion injury, Exp. Mol. Med. 54 (2) (2022) 180–193.
[58] S. Iwai, K. Kaji, N. Nishimura, et al., Glucagon-like peptide-1 receptor agonist, semaglutide attenuates chronic liver disease-induced skeletal muscle atrophy in diabetic mice, Biochim. Biophys. Acta, Mol. Basis Dis. 1869 (7) (2023) 166770.
[59] Y. Li, B. Xu, J. Yang, et al., Liraglutide protects against lethal renal ischemia-reperfusion injury by inhibiting high-mobility group box 1 nuclear-cytoplasmic translocation and release, Pharmacol. Res. 173 (2021) 105867.
[60] M. Malm-ErjefäLT, I. BjøRNSDOTTIR, J. Vanggaard, et al., Metabolism and excretion of the once-daily human glucagon-like peptide-1 analog liraglutide in healthy male subjects and its in vitro degradation by dipeptidyl peptidase IV and neutral endopeptidase, Drug Metab. Dispos. 38 (11) (2010) 1944–1953.
[61] J. Moellmann, B.M. Klinkhammer, J. Onstein, et al., Glucagon-like peptide 1 and its cleavage products are renoprotective in murine diabetic nephropathy, Diabetes 67 (11) (2018) 2410–2419.
[62] T. Guo, W. Yan, X. Cui, et al., Liraglutide attenuates type 2 diabetes mellitus-associated non-alcoholic fatty liver disease by activating AMPK/ACC signaling and inhibiting ferroptosis, Mol. Med. 29 (1) (2023) 132.